

# **SUN SENSORS FOR SMALL SATELLITES ATTITUDE DETERMINATION SYSTEMS**

**A Degree Thesis  
Submitted to the Faculty of the  
Escola Tècnica d'Enginyeria de Telecomunicació de  
Barcelona  
Universitat Politècnica de Catalunya  
by  
Álvaro Enrich Carmona**

**In partial fulfilment  
of the requirements for the degree in  
TELECOMMUNICATIONS SYSTEMS ENGINEERING**

**Advisor: Professor Adriano José Camps Carmona**

**Barcelona, June 2017**

## **Abstract**

It is more and more obvious that nanosatellites are becoming key players to conduct all kinds of experiments; most of which will lead to the development of larger and more powerful systems, once the aforementioned nanosatellites experiments are proven valid. The ‘Teoria de la Senyal i les Comunicacions’ department of the Universitat Politècnica de Catalunya is currently developing and studying CubeSats for technology demonstration and as platforms of small scientific experiments. Given the fact that the satellite structure and capacity are not without limitations, all projects have to contemplate them to fulfill the requirements. Consequently, in this thesis, more economic devices that will also not take that much space in the nanosatellite are considered.

This degree thesis presents the development of the whole Sun sensor subsystem of <sup>3</sup>CAT-4, the next UPC’s NanoSat Lab project. The circuit implementing the system is the same as the one that was previously designed in the “Projecte Avançat d’Enginyeria” subject. However, the integration in the CubeSat, the software to communicate with the on board computer and the estimation data software are implemented from scratch. The calibration system is improved, considering it was previously designed, and the software to perform it is also implemented from scratch.

Overall, this thesis sheds light on how to develop a low-cost Sun sensor for a nanosatellite and the constrains that have to be taken into account when doing so.

## **Resum**

Cada cop més, resulta obvi que els nanosatèl·lits estan sent l'impuls per dissenyar tot tipus d'experiments que puguin arribar a desenvolupar sistemes molt més potents, un cop provats i especialitzats els anteriors. El departament de Teoria del Senyal i les Comunicacions de la Universitat Politècnica de Catalunya està actualment estudiant i desenvolupant CubeSats per tal de demostrar tot tipus de tecnologies i com a plataformes per a petits experiments científics. Tenint en compte el fet que la pròpia estructura i la capacitat del satèl·lit suposen certes limitacions, tots els projectes les han de contemplar a l'hora de satisfer els seus requisits. En conseqüència, en aquesta tesi, són considerats els dispositius més econòmics i que puguin aprofitar al màxim l'espai dels nanosatèl·lits utilitzats.

En aquest projecte es desenvolupa completament un subsistema “Sun Sensor” per al proper projecte del NanoSat Lab de la UPC, el <sup>3</sup>CAT-4. El circuit electrònic que implementa el sistema és el mateix que el dissenyat prèviament a l'assignatura de Projecte Avançat d'Enginyeria. No obstant, la integració del sistema al CubeSat, el software de comunicació amb l'ordinador a bord i el procés d'estimació de la direcció de la llum incident es dissenyen i implementen de zero. El sistema mecànic de calibratge es millora, ja que ja existia una primera versió dissenyada però el software per dur a terme el calibratge del sensor també s'implementa des de zero.

En general, aquesta tesi dóna llum a com desenvolupar un “Sun sensor” de baix cost per nanosatèl·lits i les restriccions que s'han de tenir en compte per fer-ho.

## **Resumen**

Cada vez resulta más obvio que los nanosatélites están siendo el impulso para diseñar todo tipo de experimentos que puedan llegar a desarrollar sistemas mucho más potentes, una vez probados y especializados los anteriores. El departamento de "Teoria de la Senyal i les Comunicacions" de la Universitat Politècnica de Catalunya está actualmente estudiando y desarrollando CubeSats para demostrar todo tipo de tecnologías y como plataformas para pequeños experimentos científicos. Teniendo en cuenta el hecho de que la propia estructura y la capacidad del satélite suponen unas limitaciones, todos los proyectos deben contemplarlas para satisfacer sus requisitos. En consecuencia, en esta tesis, son considerados los dispositivos más económicos y que puedan aprovechar al máximo el espacio de los nanosatélites usados.

En este Proyecto se desarrolla completamente un subsistema "Sun sensor" para el próximo proyecto del NanoSat Lab de la UPC, el <sup>3</sup>CAT-4. El circuito electrónico que implementa el sistema es el mismo que el diseñado previamente en la asignatura de "Projecte Avançat d'Enginyeria". Sin embargo, la integración del sistema en el CubeSat, el software de comunicación con el ordenador de a bordo y el proceso de estimación de la dirección de la luz incidente se diseñan e implementan de cero. El sistema mecánico de calibración se mejora, ya que existía una primera versión diseñada, pero el software para llevar a cabo la calibración también se implementa de cero.

En general, esta tesis da luz a como desarrollar un "Sun sensor" de bajo coste, para nanosatélites y las restricciones que deben tenerse en cuenta para llevarlo a cabo. e



*To all of my family.*

## **Acknowledgements**

First of all, I would like to express my gratitude to my advisor Prof. Adriano Camps for being always available to answer my questions and helping me to go through this last semester. His help to develop this project and to improve this report was essential to conclude this thesis, and he also believed in my abilities giving me the opportunity to learn more about the space sector working on the <sup>3</sup>CAT-4 project.

I would like to thank all the members of the UPC's NanoSat Lab for the support given and the good work environment.



## **Revision history and approval record**

<b>Revision</b>	<b>Date</b>	<b>Purpose</b>
0	31/05/2017	Document creation
1	dd/mm/yyyy	Document revision

### DOCUMENT DISTRIBUTION LIST

<b>Name</b>	<b>e-mail</b>
Alvaro Enrich	<a href="mailto:alvaroenrich@gmail.com">alvaroenrich@gmail.com</a>
Adriano Camps	<a href="mailto:camps@tsc.upc.edu">camps@tsc.upc.edu</a>

Written by:		Reviewed and approved by:	
Date	31/05/2017	Date	28/06/2017
Name	Alvaro Enrich	Name	Adriano Camps
Position	Project Author	Position	Project Supervisor

## Table of contents

<b>Abstract .....</b>	<b>II</b>
<b>Resum .....</b>	<b>III</b>
<b>Resumen .....</b>	<b>IV</b>
<b>Acknowledgements.....</b>	<b>VI</b>
<b>Revision history and approval record.....</b>	<b>VII</b>
<b>Table of contents.....</b>	<b>VIII</b>
<b>List of Figures.....</b>	<b>X</b>
<b>List of Tables: .....</b>	<b>XII</b>
<b>1. Introduction.....</b>	<b>1</b>
1.1. Background .....	1
1.2. Main constraints.....	1
1.3. Sun sensor subsystem.....	2
1.3.1. Photodiode.....	2
1.3.2. Data processing .....	2
1.3.3. Calibration system .....	3
1.4. Work plan, milestones and Gantt .....	3
<b>2. State of the art of the technology used or applied in this thesis: .....</b>	<b>4</b>
<b>3. Methodology / project development: .....</b>	<b>5</b>
3.1. System Design .....	5
3.2. Hardware Design.....	5
3.3. Software Design.....	11
3.3.1. Data processing .....	11
3.3.2. I2C Communication Protocol .....	14
3.4. Calibration Process .....	17
<b>4. Results.....</b>	<b>22</b>
4.1. Vacuum Test.....	22
4.2. Cover.....	24
4.3. Calibration Results .....	24
<b>5. Budget.....</b>	<b>28</b>

<b>6. Conclusions and future development:</b>	<b>29</b>
<b>Bibliography:</b>	<b>XIII</b>
<b>Appendices:</b>	<b>XIV</b>
<b>    Appendix A: Work Plan Packages, milestones and Gantt Diagram</b>	<b>XIV</b>
<b>    Appendix B: Matlab system simulation</b>	<b>XIX</b>
<b>    Appendix C: Circuit Design</b>	<b>XXIV</b>
<b>    Appendix D: Circuit simulation</b>	<b>XXIX</b>
<b>    Appendix E: Estimation Process</b>	<b>XXXIII</b>
<b>    Appendix F: Calibration process</b>	<b>XXXV</b>
<b>    Appendix G: System Requirements</b>	<b>XXXIX</b>
<b>Glossary</b>	<b>XLI</b>

## List of Figures

Figure 3.1 – Prototype of container box .....	6
Figure 3.2 – Sun sensor circuit Schematic.....	7
Figure 3.3 – PCB Design.....	7
Figure 3.4 – PCB Hole Design and both PCB mounted .....	8
Figure 3.5 – Design of the cover to be plotted on the film .....	9
Figure 3.6 – Cover of the photodiode plotted .....	9
Figure 3.7 – Final version of vacuum system .....	10
Figure 3.8 – Prototypes with the cover placed .....	11
Figure 3.9 – Mean approximation error for a 9 <sup>th</sup> order polynomial.....	12
Figure 3.10 – Relationship between polynomial length and mean error .....	13
Figure 3.11 – Relationship between mean error and computational time .....	14
Figure 3.12 – Flow diagram for the L053R8 microcontroller .....	16
Figure 3.13 – Configuration call I2C header.....	17
Figure 3.14 – Mechanical system to calibrate the sensor. ....	18
Figure 3.15 – Drivers PCB .....	19
Figure 3.16 – Flow diagram of the calibration process.....	20
Figure 3.17 – Axes rotations for the calibration mechanical system (left) and the sensor light detection system (right) .....	20
Figure 4.1 – OPR5911 High vacuum warning .....	22
Figure 4.2 – Thermal Vacuum Chamber .....	23
Figure 4.3 – Results of silver mirroring process in a coverslip .....	24
Figure 4.4 – Prof. Pablo Ortega's Sun simulator and NanoSat Lab's Sun simulator .....	25
Figure 4.5 – Final Calibration system .....	26
Figure 4.6 – Estimation error with real calibration data .....	27
Figure A.1 – Gantt Diagram .....	XVIII
Figure B.1 – Top view of the system simulated .....	XIX
Figure B.2 – Angles used in the simulation .....	XX
Figure B.3 – Illuminated area of each photodiode for each of the possible angles .....	XX
Figure B.4 – Illuminated area of one photodiode .....	XXI
Figure B.5 – Spectral Responsivity of the OPR5911 .....	XXII
Figure B.6 – Output current for each photodiode for all the possible angles .....	XXIII
Figure C.1 – Equivalent Circuit of a photodiode .....	XXV
Figure C.2 – Pin configuration and physical dimensions of the OPR5925 model .....	XXV
Figure C.3 – Top view of the pin configuration for the S6 package model.....	XXVI
Figure C.4 – Recommended configuration of the LT6654 .....	XXVI

Figure C.5 – Physical connections of the GN Package 16-Lead, with the 4 AO's sharing the V+ and V- supplies .....	XXVI
Figure C.6 – Filter design .....	XXVII
Figure C.7 – Schematic of the circuit for each photodiode.....	XXVIII
Figure D.1 – Output voltage difference due to temperature variations .....	XXIX
Figure D.2 – Final design of the filter including the 1 $\mu$ F capacitor .....	XXX
Figure D.3 – Filter response in frequency domain .....	XXX
Figure D.4 – Filter response in temporal domain .....	XXXI
Figure D.5 – First design with the resistors in parallel .....	XXXI
Figure D.6 – Filter response in frequency domain .....	XXXII
Figure F.1 – Schematic of the drivers' circuit .....	XXXV
Figure F.2 – Piece used to attach the PCB to the calibration machine .....	XXXVI
Figure F.3 – First 3D piece attached to the calibration machine .....	XXXVII
Figure F.4 – 3D view of the final piece .....	XXXVIII

## **List of Tables:**

Table 2.1 – Comparison of different Sun sensors available in the market .....	4
Table 3.1 – Priority relation to data delay .....	17
Table 4.1 – Vacuum test results.....	23
Table C.1 – Electrical characteristics extracted from the datasheet .....	XXIV
Table G.1 – Requirements Glossary .....	XXXIX
Table G.2 – System Requirements .....	XL

## 1. Introduction

This chapter contains a short introduction to the CubeSat concept and the UPC's NanoSat Lab. It also includes the main constraints when designing and developing a CubeSat and an analysis of the current state of the project.

### 1.1. Background

The CubeSat standard was developed in 1999 by Bob Twiggs and Professors Jordi Puig-Suari. In the standard, it was specified that a CubeSat should fit in a Poly-Picosatellite Orbital Deployer, a standardized launcher. This P-POD was standarized in order to deploy between one to three spacecrafts, with a total size no larger than 10 cm x 10 cm x 33 cm. Therefore, the standard dimensions for a CubeSat are 10 cm x 10 cm x 11 cm, also called one unit [1].

The UPC NanoSat Lab has been involved in several nanosatellite projects and missions, such as <sup>3</sup>CAT-1, <sup>3</sup>CAT-2, <sup>3</sup>CAT-3, and now <sup>3</sup>CAT-4. These missions have not only required the implementation of nanosatellites, but also their designs according to their very specific requirements. These tasks are being carried out by a group of students, which divide their tasks, design their subsystems, test them and finally work as a team to integrate everything in the nanosatellite.

This project's main goal is to develop the Sun sensor subsystem for <sup>3</sup>CAT-4, which should be compliant with <sup>3</sup>CAT-3. <sup>3</sup>CAT-4 mission born in response to the ESA call of the Fly Your Satellite in December 2016. This program offered European universities the possibility to launch their CubeSats from the International Space Station in collaboration with the ESA. Therefore, after reading the requirements to apply, it was decided to start a new satellite, called <sup>3</sup>CAT-4, which would inherit many subsystems or solutions from its predecessors. During the development of this thesis, the <sup>3</sup>CAT-4 project has been selected to be launched.

### 1.2. Main constraints

The main constraint of any CubeSat project is related to the size and mass of the spacecraft. The size will define most of the physical requirements of the project. The CubeSat standard specifies that a CubeSat unit must have a maximum mass of 1 kg. This constraint will have huge impact when taking into account the materials used [2].

The electrical power system of a CubeSat generates, stores, controls and distributes the electrical power. Power demands beginning-of-life and end-of-life must be taken into consideration, in order to enable the EPS to fulfill its top level functions. Top level functions are mainly, supplying a continuous source of electrical power to the satellite bus during the mission lifetime, control and distribute power to the and to provide power during periods of average and peak power demand [3].

### **1.3. Sun sensor subsystem**

The Sun position can be estimated using “Sun sensors”. This subsystem gives as an output the direction of the incident light. This subsystem is included in a much more complex subsystem, the Attitude Determination Control System (ADCS).

The aim of the ADCS is to control the stabilization of the CubeSat for many reasons, for example the antenna may be accurately pointed to the Earth for good communications’ performance, so that the experiments’ data can be correctly interpreted.

#### **1.3.1. Photodiode**

The Sun sensor hardware has a photodiode to collect data. The photodiode is the component that will have an output proportional to the incident light on its surface. The component used, is not a common photodiode, it is actually a  $2 \times 2$  array of photodiodes. The main requirement that the system has to meet regarding the incident light, is to detect its direction with an error not larger than  $1^\circ$ . However, the photodiodes alone do not have this resolution, so the initial idea was to partially cover the photodiodes with a film in order to get a higher resolution.

The next step is to finally design this cover, which should be glass made and reflective everywhere, except in the part where the light shall pass, and design a way to insert this system in the CubeSat.

#### **1.3.2. Data processing**

The photodiode will give an output proportional to the incident light, but this output must be processed. This output will be a current, which must be converted into voltage in order to be processed with an analog to digital converter. A circuit to perform this function was designed by a Mr. Hector Esteban and I during the ‘Projecte Avançat d’Enginyeria’ subject, but all the processing software had to be done.

This software will be responsible for reading the data from the circuit, obtaining the incident light for it and finally send it to the microcontroller.

### 1.3.3. Calibration system

Finally, the calibration system must be implemented too. This system is responsible for the calibration of each sensor once they have been integrated within the nanosatellite, since it is possible that the cover of the photodiodes have small differences from one sensor to the other. The system will be composed of two main parts, the hardware (a printed circuit board attached to an Arduino UNO board) and the software, which will control the Arduino and the Sun sensor microcontroller.

### 1.4. Work plan, milestones and Gantt

The information concerning this section can be found in Appendix A.

## **2. State of the art of the technology used or applied in this thesis:**

This section aims to provide a quick overview on research performed for Sun sensors for spacecrafts and CubeSats.

The Sun sensor designed in this thesis is based in the same idea as most of the Sun sensors that are currently available in the market. Most of them perform the sunlight direction determination using two orthogonal axes, as the one designed in this thesis. Their Field Of View (FOV) is usually around  $\pm 60^\circ$ , another characteristic of the system described in this thesis. Most of them also use the technique of having a cover, in order to obtain the accuracy required. Some of the main characteristics of some Sun sensors available in the market can be found in Table 2.1.

Table 2.1 – Comparison of different Sun sensors available in the market

Sensor	Field of View	Axes	Accuracy	Dimensions	Mass	Price
Nano-SSOC-A60	$\pm 60^\circ$	2 orthogonal	$<0.5^\circ$	27.4 x 14 x 5.9 mm	4 g	2200 €
NanoSSOC-D60	$\pm 60^\circ$	2 orthogonal	$<0.5^\circ$	43 x 14 x 5.9 mm	6.5 g	3600 €
NSS CubeSat Sun Sensor	$\pm 57^\circ$	-	$<0.5^\circ$	33 x 11 x 6 mm	<5 g	3300 €
NSS Fine Sun Sensor	$\pm 70^\circ$	-	$<0.1^\circ$	34 x 32 x 21 mm	35 g	12000 €
SSOC-A60	$\pm 60^\circ$	2 orthogonal	$<0.3^\circ$	30 x 30 x 12 mm	25 g	7200 €
SSOC-D60	$\pm 60^\circ$	2 orthogonal	$<0.3^\circ$	60 x 30 x 12 mm	35 g	12200 €

### **3. Methodology / project development:**

After the description of the background, this chapter explains the design and implementation of the different parts of the Sun sensors subsystem. This includes, the hardware design, the software design and implementation and the calibration process.

#### **3.1. System Design**

The system has been designed and divided into three main parts. Hardware design, software design and calibration process.

The first part includes the circuit design, which was previously implemented during the ‘Projecte Avançat d’Enginyeria’ subject. It also includes the Printed Circuit Board (PCB) design, the cover design, and what is more important, integrating physically the subsystem in the whole CubeSat. This last part, integrating the whole subsystem in the CubeSat, will be fully determined by the final design of the cover and its attaching system. This is the most critical part of this section of the system, since this will condition all the PCB design.

The second part is the software design and it includes all the processing software to obtain a good estimation of the angles given the 4 outputs of the photodiodes. It also includes the communication protocol between the Sun sensor microcontroller and the On Board Computer (OBC). All these tasks will include simulations to decide which is the best estimation option, in terms of error, computational time and power.

The calibration process is a procedure that must be done before launch once the Sun sensor is integrated in the CubeSat. Therefore, the calibration is an extremely important part, since a bad calibration will directly lead to a bad performance of the Sun sensor during the mission. The calibration main tasks are to implement the software that will move the calibration system and the hardware that will control the stepper motors.

#### **3.2. Hardware Design**

The first idea for the integration of the subsystem with the CubeSat consisted of a box containing the sensor, the circuitry, and the microcontroller, with two apertures, one for the cover of the sensor and one for the communications with the OBC, as it can be seen in Figure 3.1. Therefore, the goals for the system using this design are to create the smallest design possible, to contain it in the box and make it fit.

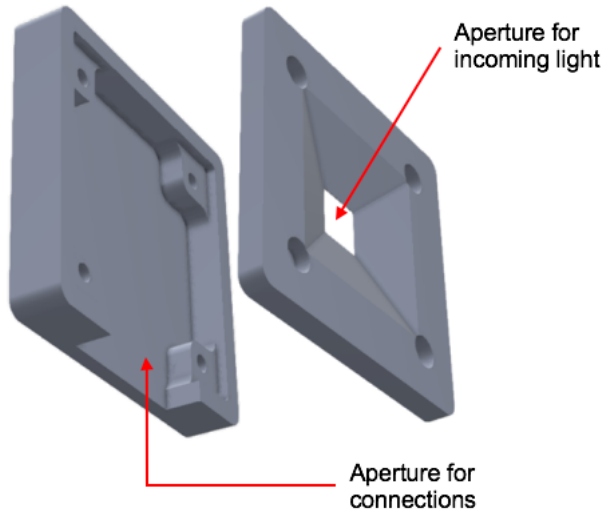


Figure 3.1 – Prototype of container box

Therefore, with the box design that was made, the PCB design that was made was a 1-inch x 1-inch PCB implementing the designed circuit to obtain the four output voltages. As it can be seen in Figure 3.3, this is a two-layer PCB. In one layer, there is only the photodiode, which is the only component that will be exposed. All the other components are in the other layer, and it is especially important to note that the quad operational amplifier is not under the photodiode, but next to. This design feature is applied due to the low output current given by the photodiode. Since the current is on the order of  $\mu\text{A}$ , and internal resistance of the wiring can affect it severely. Therefore, to minimize the possibility of this internal resistance or capacitance affecting this low current signal, the best option is to have the route as short as possible.

The circuit design is shown in Figure 3.2. This circuit has 3 main blocks, the LT6654-3, the OPR5911 and the LT6005HGN. The first one is a 3V voltage regulator, the second one is the 2x2 array of photodiodes and the last one is the quad-op-amp integrated circuit. This circuit behaves as 4 independent circuits, one for each photodiode. The regulator supplies a common voltage, and then each of the photodiodes will receive the incoming light, and with the amplifier configured correctly, will convert the output current into an output voltage

$$V_{out} = 3 - R_f \cdot I_{ph} \quad (3.1)$$

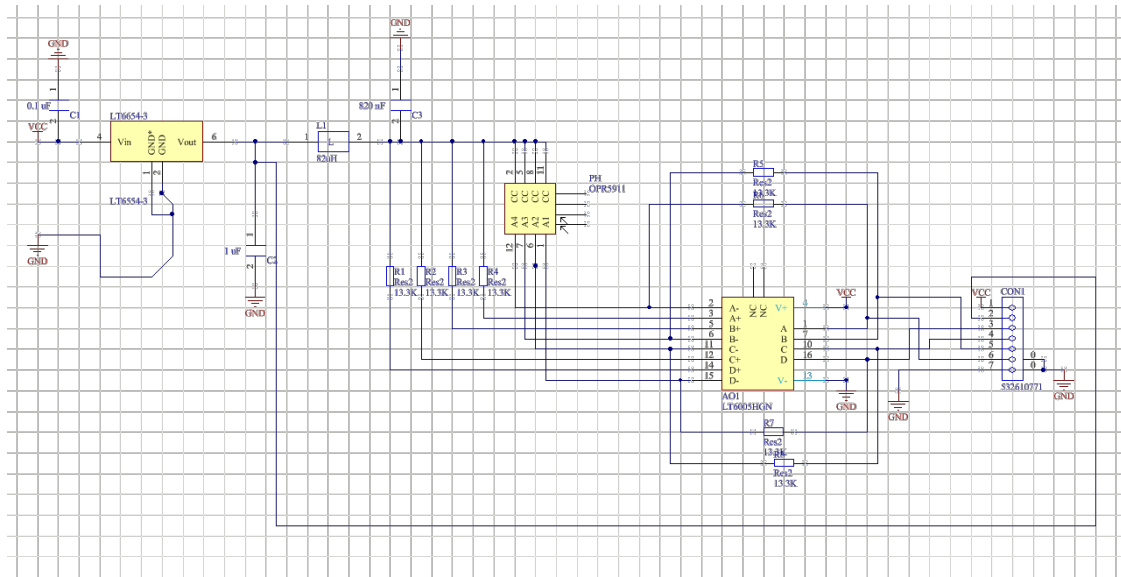


Figure 3.2 – Sun sensor circuit Schematic

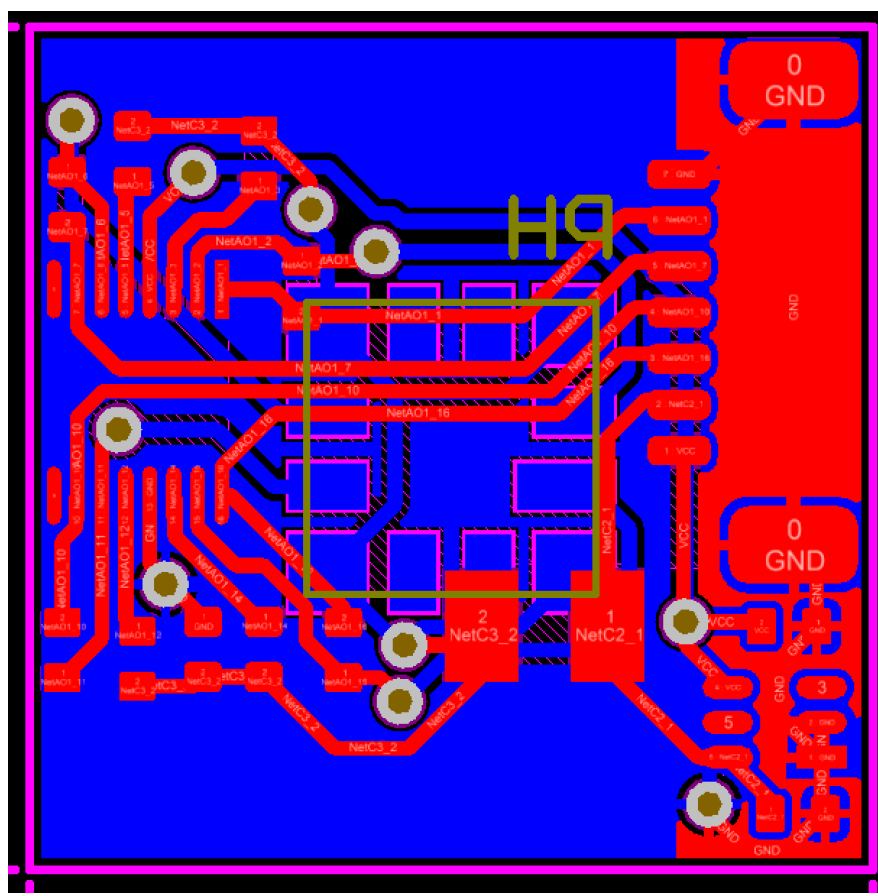


Figure 3.3 – PCB Design

Once the PCB has been designed, the next step is the integration of all the system in the CubeSat. The box solution proposed in Figure 3.1 was not compliant with the requirements, since it is too large. Therefore, the solution to the integration problem

taking into account the size requirement is the following. This solution consisted of redesigning the solar panel's PCB to make an aperture in it. This aperture should have the same exact size of the photodiode, so that everything but the photodiode is covered. Therefore, the final system would physically look to something similar to what can be seen in Figure 3.4, with all the solar panels that are not in the prototype.

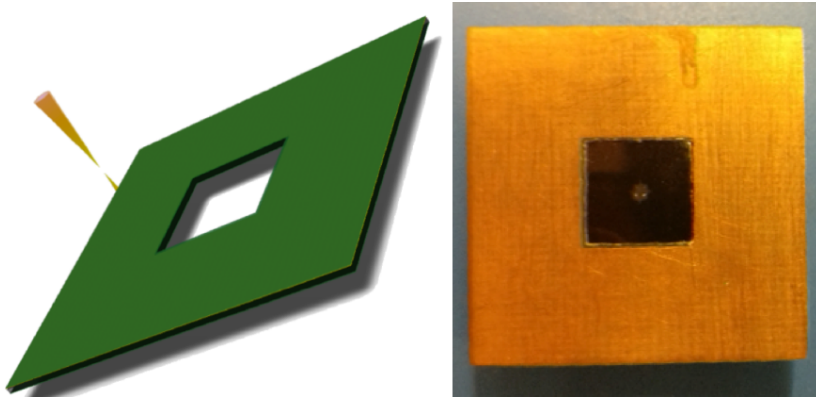


Figure 3.4 – PCB Hole Design and both PCB mounted

This design was compliant with the project requirements, and once arrived at this point there was only one more thing to worry about concerning physical or hardware design: the cover. The main constraint on the cover design is its thickness. It would not make any sense to have a thick cover. It can only protrude up to 1 mm [4][5]**Error! No se encuentra el origen de la referencia..** Therefore, in the 'Projecte Avançat d'Enginyeria' subject, a prototype with a photo plotter film was made, but there was not a good system designed to fix it. Taking into account that the new integration system did not have a box, the best option to fix it, was to design the cover with the exact same size as the photodiode, and attach it with silicone. At this point it was noticed that in order to attach something with silicone, it would be better if it was glass made, and it was decided to try to make it reflective, so there was no possibility for the light to filter. Glass fitted with all the requirements that had been set. Glass is rigid enough to avoid bending when fixing it with silicone, and it can be painted with reflective ink, or it can be mirrored. Therefore, in order to make a reflective cover, it was decided to purchase a really thin glass. The glass used has been a typical coverslip for a microscope. In order to make it reflective, the sputtering machine idea was considered, but it was way too expensive for the initial idea and the budget allocated to this subsystem. Then, after some research, a possible solution was the silver mirroring. In order to mirror a glass, the tollens' reagent can be used. Therefore, to perform this mirroring, some chemicals were purchased: silver nitrate, glycerin, ammonia and sodium hydroxide. With these chemicals, it was possible to use

the reagent for silver mirroring. However, after many attempts that will be shown in the results section of the thesis, it was decided to go for a provisional solution, since the experiment was unsuccessful. The film solution made with the photo plotter, looked as the best option, as a temporal solution. For further developments, the possibilities of using a sputtering machine or performing a good mirroring using the tollens' reagent experiment with an expertise in chemistry were considered, since there are other possibilities with other chemicals[6].

The final design applied to the cover with the photo plotter is shown in Figure 3.5.

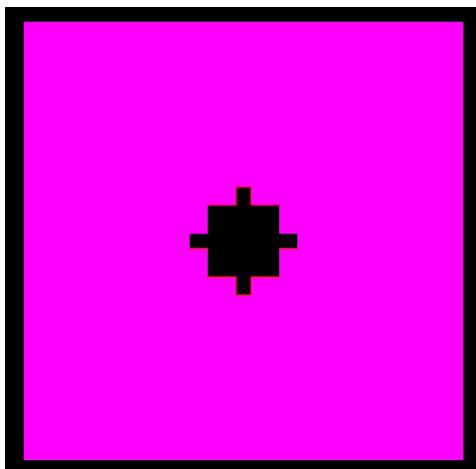


Figure 3.5 – Design of the cover to be plotted on the film

Where, as it can be seen in Figure 3.6, the pink part of Figure 3.5 is plotted in black in the film, being this the opaque part, and the black part in Figure 3.5 is the aperture through which the sunlight excites the photodiodes.

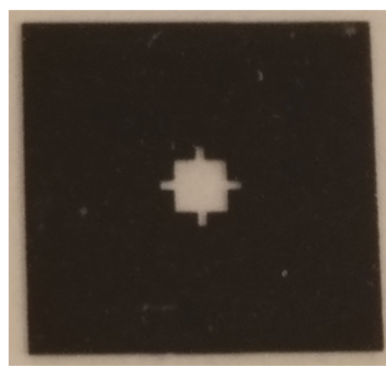


Figure 3.6 – Cover of the photodiode plotted

The idea to attach the cover was to use solar panels silicone. This silicone is created using the SYLGARD 184 Silicone Elastomer. As explained in the product data file, in order to obtain a good bonding, it is necessary to mix the two products included in the kit. These two products are the base and the curing agent, and the mix must be 10 parts of

base, and 1 part of curing agent. Then, when mixing, the silicone is obtained, and in order to make it solid it is necessary to heat it at 60 degrees during 45 minutes. However, while mixing the silicone, many bubbles appear. These bubbles must be removed before placing the cover on the silicone, due to the fact that bubbles will expand in vacuum and explode in space conditions. Then, these bubbles must be removed. To do so, since it is such a dense mix, it is necessary to apply vacuum to it, in order to make the bubbles grow and explode. Therefore, to perform the vacuum, a small vacuum chamber was designed, but results were unsuccessful. Therefore, the final chamber used was a cylindrical one, that was already available in the laboratory. This vacuum system is shown in Figure 3.7.

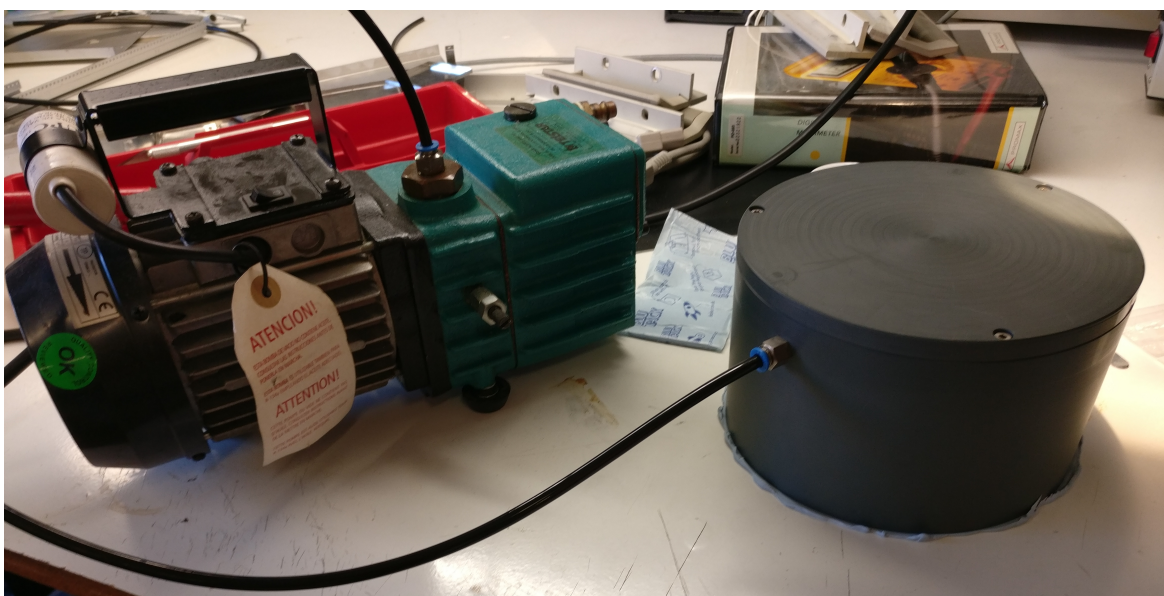


Figure 3.7 – Final version of vacuum system

This chamber was sealed using a pressure-sensitive adhesive, which worked perfectly, but every time had to be placed correctly again. Then, the bubbles were removed, the silicone was applied to the photodiode, and the cover was placed with the microscope. After that the vacuum was applied again, to avoid possible bubbles that may have appeared during the placing. Finally, the system was put in the oven, and the cover was correctly fixed.

In Figure 3.8 an image of the placing can be found. As it can be seen, the cover is not perfectly symmetric with the 4 little dots that can be seen in the center of the photodiode. This clearly denotes a placing error, although the calibration process should be able to correct this.

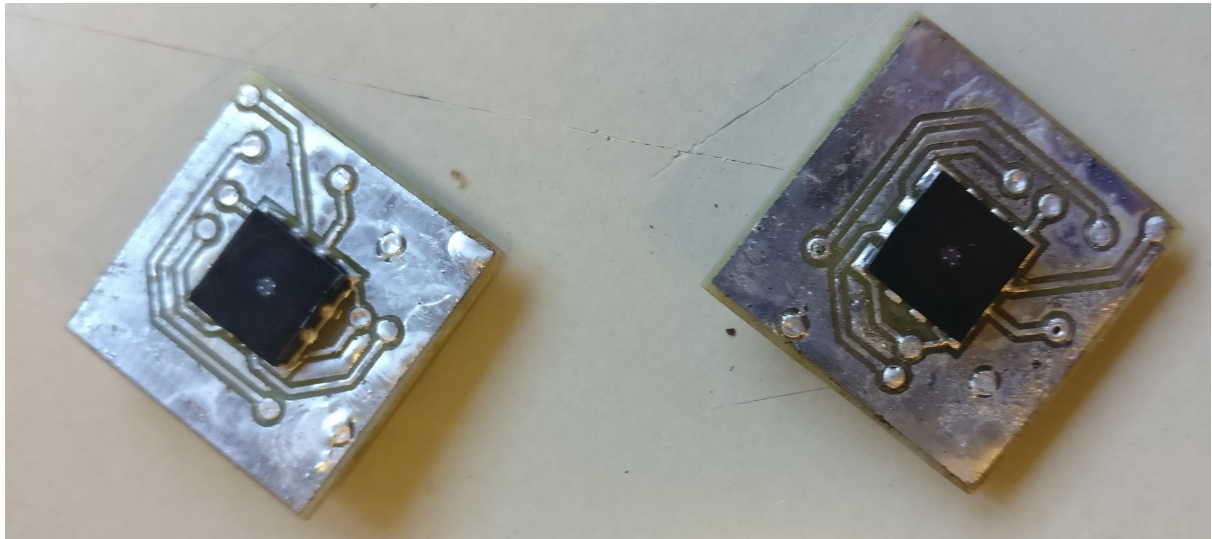


Figure 3.8 – Prototypes with the cover placed

### 3.3. Software Design

#### 3.3.1. Data processing

As previously explained, this part of the subsystem is responsible for obtaining the 4 inputs from the circuit and transform them into the sunlight direction. To do so, the first idea was to calibrate the system in order to obtain lookup values. However, with the accuracy required, at least four  $360 \times 61$  lookup tables were required, all of them loaded with `uint16_t` variables. An `uint8_t` variable is not a valid option because it can only represent values from 0 to 255, and the ADC values of the microcontroller have a 12-bit resolution, what means a range from 0 to 4095. Therefore, the number of bytes to represent an integer that can cover all the range is two, what means 16 bits. Then the final size of the total data to load to the microcontroller is computed as:

$$\begin{aligned} \text{Size} &= \text{NumOfTables} \cdot \text{SizeOfTable} \cdot 2 \text{ bytes} \\ \text{Size} &= 4 \cdot 360 \cdot 61 \cdot 2 \text{ bytes} = 175.68 \text{ KB} \end{aligned} \tag{3.2}$$

Since the idea was to load it into a STM32 L053R8 microcontroller, which has a 64 KB flash memory, it is not possible to load this large amount of data. However, by performing an estimation this problem was solved, and, by using the ordinary least squares, it was possible to obtain two estimations of the Direction Of Arrival (DOA) angles,  $\theta$  and  $\phi$  [7].

$$\begin{aligned} \theta_{coeff} &= P * \theta \\ \phi_{coeff} &= Q * \phi \end{aligned} \tag{3.3}$$

As it can be seen, by using the OLS estimation [8], it is possible to obtain two arrays of coefficients of theta and phi, where P and Q are matrices called the Moore–Penrose pseudo-inverse, and  $\theta$  and  $\phi$  are the arrays of samples. Then, given the 4 measurements from the 4 photodiodes, it is possible to obtain a polynomial approximation of any order, in order to estimate the incidence angles, theta or phi. The only thing left to do, is to multiply the polynomial coefficients by  $\theta_{\text{coeff}}$  or  $\phi_{\text{coeff}}$ . In Appendix E more information about the estimation process can be found.

Therefore, with this code it is possible to obtain an estimation of the angle, without having to load that big amount of data. However, the amount of data to be loaded cannot be specified yet, since it will depend on the polynomial order.

$$\text{Data Size} = 2 * \text{PolyLength} * 4 \text{ bytes}$$

(3.4)

There are two arrays of coefficients, each of them with the length of the polynomial and each field of them is a double, which has a size of 4 bytes. In order to check this approximation method, it is necessary to use a calibration matrix. However, since this was implemented before the calibration process, and by using the system simulation output matrices, the estimation method could be verified.

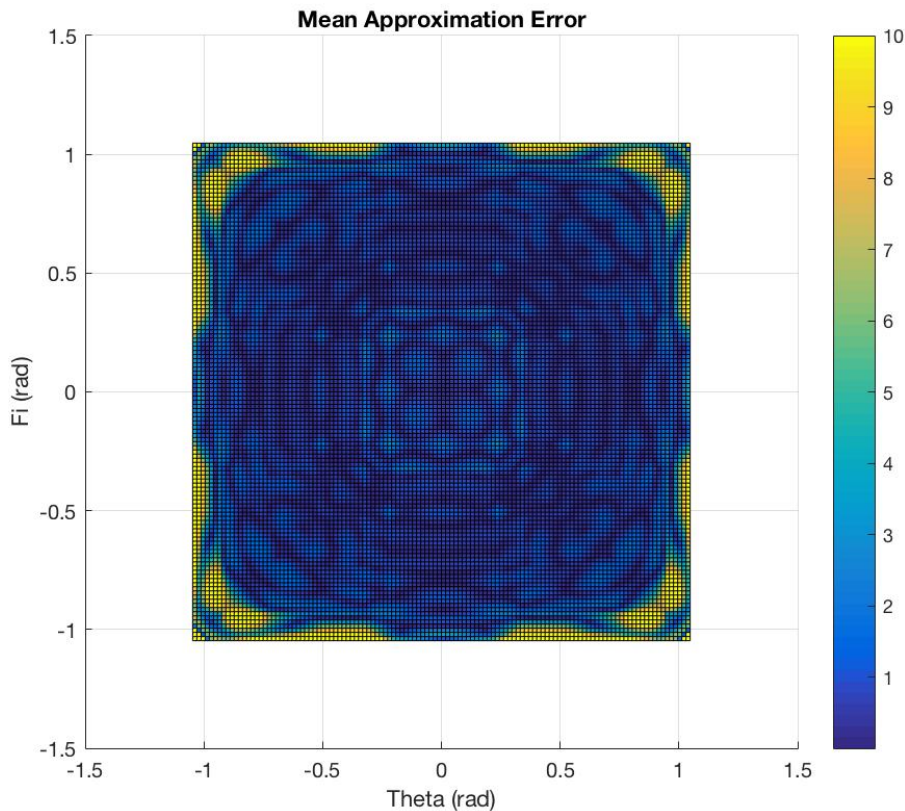


Figure 3.9 – Mean approximation error for a 9<sup>th</sup> order polynomial

As it can be seen in Figure 3.9, dark blue areas represent an error minor than  $1^\circ$ , light blue an error between  $2^\circ$  and  $4^\circ$  and yellow areas an error higher than  $8^\circ$ . This estimation was performed in all the possible orders.

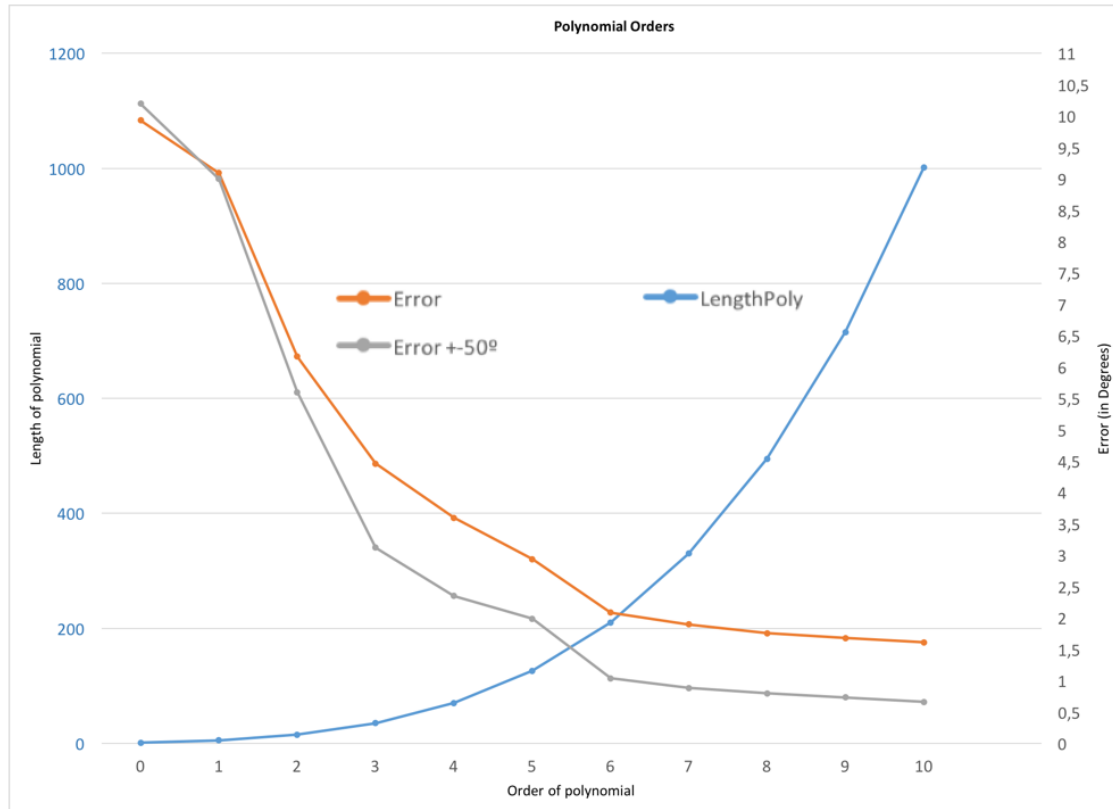


Figure 3.10 – Relationship between polynomial length and mean error

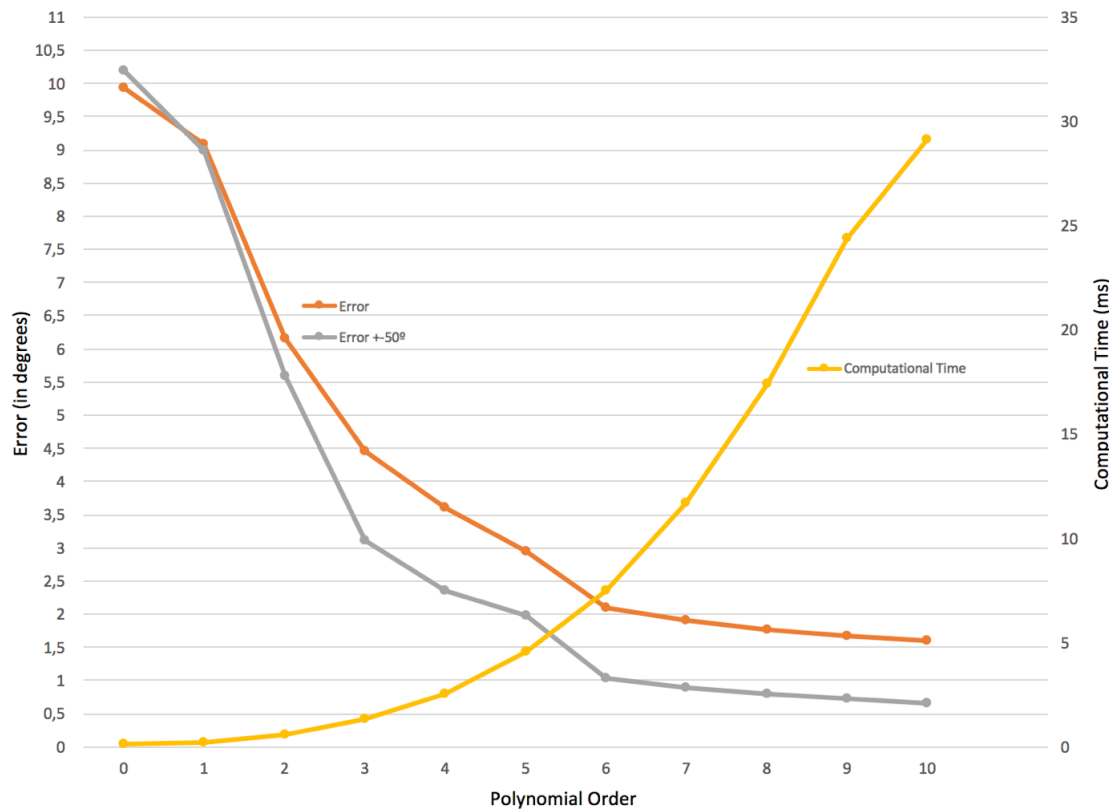


Figure 3.11 – Relationship between mean error and computational time

In Figure 3.10 and Figure 3.11 it is possible to observe the relationship between the mean error, the computational time, and the order of the polynomial. The results shown in Figure 3.10 show that a higher order will perform a better estimation. However, the improvement in the error is not constant.

In Figure 3.11, where the computational time is taken into account it is possible to see the same evolution. The error decreases as the order increases. However, the computational time increases while the order increases. Therefore, taking these two parameters into account, the conclusion arrived is that the optimum order for the estimation is 7, since it will perform a good estimation in terms of error ( $<1^\circ$  in  $\pm 50^\circ$ FOV) and computational time.

### 3.3.2. I2C Communication Protocol

Once the estimation has been performed and a valid output has been obtained, it is necessary to design a communications' protocol to create a communications interface between the Sun sensors microcontroller and the OBC. To achieve these communications, an Inter-Integrated Circuit (I2C) protocol has been designed, where the Sun sensor microcontroller acts as a slave and the OBC behaves as the master. The STM32 L053R8 has a wide variety of modes of operation. The differences between one

and another mode are mainly different peripherals enabled, what has a direct impact on the power consumption. Therefore, since it will always be much better to have a low power consumption subsystem, the microcontroller will be set in stop mode, and using interruptions it will be awakened. This microcontroller will be using the Analog to Digital Converter (ADC) peripheral. However, in order to perform the ADC conversion, the Direct Memory Access (DMA) peripheral of the microcontroller will be used. That is because after considering the polling method or the interruptions ADC methods, it was decided to use the DMA ADC mode to perform the conversion. This was due to the fact that with the polling method it was not possible to read several values with a single ADC. The interruptions' method was not a suitable solution because it is not likely to be used if the conversions are going to be periodic, which is the idea of the system. Therefore, the DMA method was the method that fitted best the system needs. The L053R8 will not only use these peripherals, but it will also use the I2C peripheral. The I2C peripheral will be given interrupt permission, in order to enable the I2C interruptions. It has been decided to use the I2C peripheral with interruptions because it is the adequate way to wake up the microcontroller from a low power consumption mode and make it do its corresponding tasks. These tasks are mainly to read data from the Sun sensor, use it to estimate the incident light angle, and send all this data (both raw data and estimated angles) to the OBC, as quickly as possible and as updated as possible.

Therefore, given this situation, there were two low power consumption alternatives in order to perform the tasks correctly. The first option was to get two interrupts via I2C on the microcontroller coming from the OBC. The first interruption would order the microcontroller to read and perform the estimation process, and the second interruption would request the data. This method was satisfactory in terms of the low-power restriction and the data delay. However, the fact that the OBC had to send two I2C commands was not optimum. Therefore, the other option was to get only one interrupt via I2C, requesting the data. This opened two possibilities of development. The first possibility was to wake up the microcontroller after the request was received, read from the ADC, perform the estimation process, and then respond to the request with the data. This possibility was satisfactory in the low-power restriction, but the main problem with this solution was that the whole process would be waiting the data while it would be processed, which would suppose a delay in the data. Therefore, it was decided to implement the following possibility with one I2C command, in order to have the response as soon as possible in the OBC. This solution behaves in the following way: the microcontroller should be in low power mode, wakes up, takes measurements, processes them, and goes back to the

corresponding low power mode periodically. Therefore, when the I2C interrupt arrives, the microcontroller must instantly respond with the last data taken and processed. A flow diagram is shown in Figure 3.12.

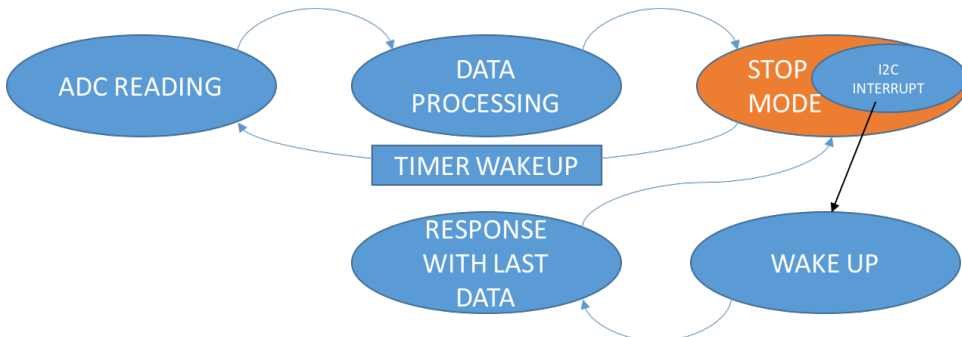


Figure 3.12 – Flow diagram for the L053R8 microcontroller

I2C headers have been designed the following way. There are two different I2C requests to the microcontroller, both of them of one-byte length, and they are identified by their MSB. In case that the MSB is high, this will mean that the call is a configuration call, and in case it is 0, it will be a request data call. This last case does not take more bits into account, since all it will do is trigger an interruption in the microcontroller to send the last data that was measured to the on-board computer. However, as its name indicates, the configuration call, gives the possibility to the user to configure the microcontroller according to some parameters. These parameters are the following: The time expected between data request calls, and the priority that the user will be giving to the low power consumption or the data delay. What the system will do is to extract from the I2C header the number of seconds between the data request calls from the bits 1 to 5 and the priority from the bits 6 to 7. Therefore, the clock and the interruptions will be configured according to the preferences sent by the on-board configurations on the Configuration Call. However, this configuration call can be sent at any time and the system should be reconfigured according to the new preferences. A visual schema can be found in Figure 3.13.

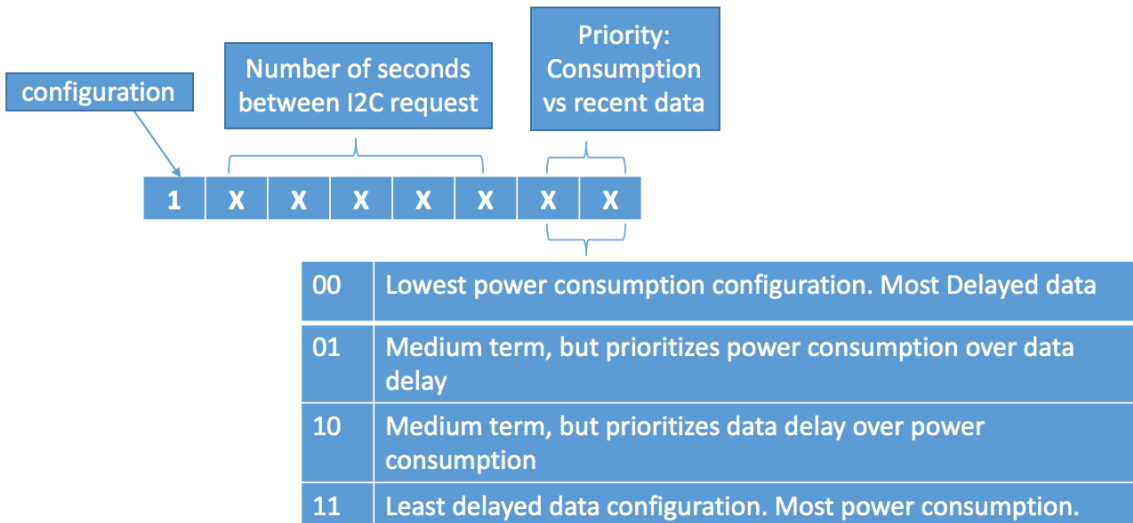


Figure 3.13 – Configuration call I2C header

The most delayed data configuration (00) will grant a delay no larger than 2 seconds. The medium term that prioritizes power consumption (01) will grant a delay no larger 1.4 seconds. The medium term that prioritizes data delay (10) will grant a delay no larger than 0.8 seconds and the last configuration (11), which prioritizes the most the least delay possible, will grant a delay no larger than 0.4 seconds.

Therefore, in summary, with the priority configuration the data delay granted will be the following:

Table 3.1 – Priority relation to data delay

Priority	Data delay
00	< 2 s
01	< 1.4 s
10	< 0.8 s
11	< 0.4 s

Therefore, by using these numbers the restriction that the OBC could not request data with a frequency higher than 4 seconds came up.

### 3.4. Calibration Process

This procedure must be done before launch, once the system is integrated in the CubeSat. It must be done with each sensor, since its main objective is to make all the sensors work properly and correct the manufacturing errors, such as for example, the error that can be done when placing the cover, which is extremely difficult to place.

Therefore, in order to calibrate the system, there are two main parts required. First of all, a solar simulator is needed in order to have the light incident on the sensor. This simulator, should be a simulator of the radiation Top Of the Atmosphere (TOA), so that the light has the same spectrum that the light is going to have in the space. The other part of the calibration process that is needed is a mechanical system that can move the sensor in order to cover all the possible directions for the light. A requirement for this mechanical system is to be able to move the sensor with at least the resolution that the sensor must have. The mechanical system used to perform the calibration system is shown in Figure 3.14, and as it can be seen, it is composed by two stepper motors, which is compliant with the requirements of covering all the sensor's FOV and taking samples within a resolution higher or equal of the one that the sensor must finally have.

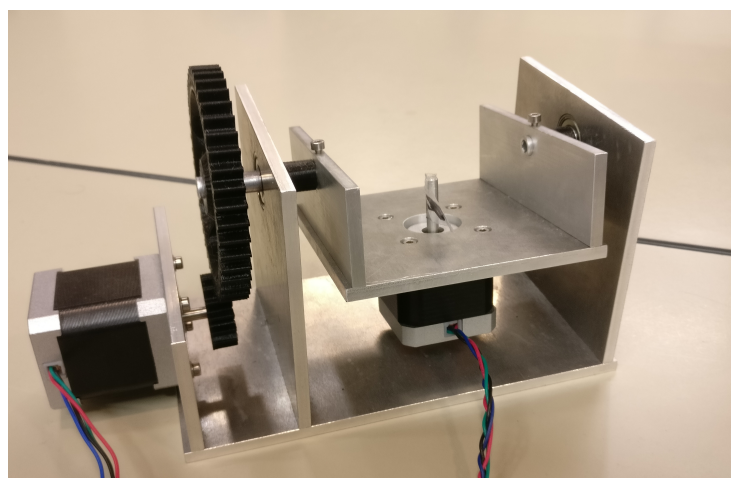


Figure 3.14 – Mechanical system to calibrate the sensor.

This system was designed a semester ago by Mr. Arnaud Solanellas, a fellow student of the Nanosat Lab. In order to move the system, an Arduino Uno board has been used, since the library `accelstepper.h` was easy to use and during the “Projecte Avançat d’Enginyeria” subject, these same steppers with Arduino were used. However, the Arduino Uno ADC’s have a 10-bit resolution, so using this ADC’s it is not possible to achieve the required resolution. Then, with this restriction, it was not possible to use the Arduino for the Analog to Digital (AD) conversion, and it was necessary to use the L053R8 to read the values from the photodiode, so there were two boards used in the process. This did not seem optimum, so it was tried to perform all the process with the L053R8 board. However, after unsuccessfully trying to control the stepper motors with the STM board, both boards were finally used. The Arduino to control the motors movement and the STM to read the photodiodes and to perform the AD conversion. In order to

control the motors properly, it was necessary to create a PCB which included a basic circuit involving two drivers to control the stepper motors, as shown in Figure 3.15.

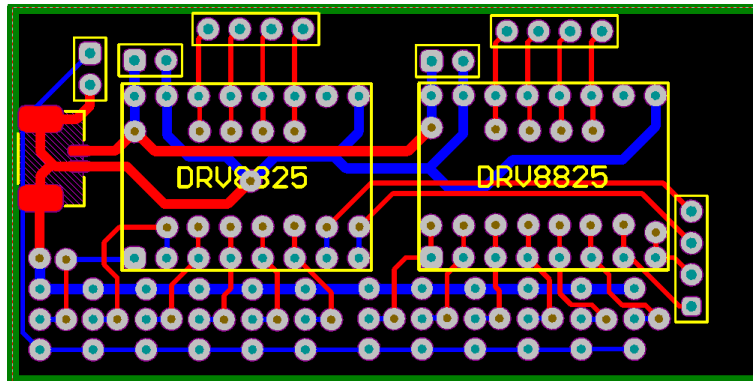


Figure 3.15 – Drivers PCB

As it can be seen, the main functionality of this PCB is to set some pins for the drivers to high or low with some jumpers, in order to have different configurations for the stepper motors. The distance between the pins for the Arduino in the PCB is the exact one in order to suit in the Arduino UNO board.

Once all this has been done, it was only necessary to develop a way to read the L053R8 board. The code implemented to do it would read a hundred times and obtain the average of the measurements, in order to have a much more accurate calibration. This code would also obtain the variance, and in case that there was a variance larger than 50, the measurements would begin again.

With all this done, the last task was to make it work all together. To do so, it was decided to implement a Matlab script that would manage the serial ports. Then, the Arduino would send a signal to the serial port informing that the position of the mechanical system is correct and it is ready to read. Then, the script would send a serial signal to the L053R8 board in order to start the reading process, which, when finished, would send the data to Matlab, that would store it and send a signal to the Arduino to move to the next position. This way, the data would also be stored in Matlab, in order to later on obtain the coefficients for the estimations of the angles. This may not seem as important as it really is, since, as may be remembered, the L053R8 does not have enough memory to store all the data for each angle.

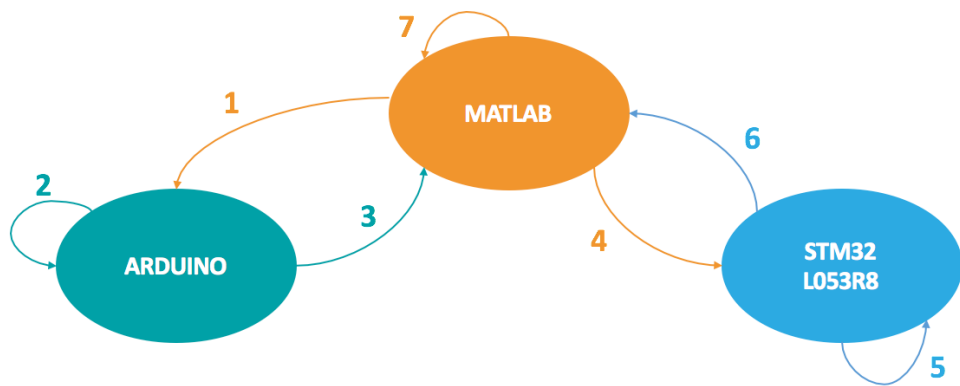


Figure 3.16 – Flow diagram of the calibration process

With this Matlab script the data is stored in Matlab, so it is ready to be processed and to obtain the estimation coefficients and the approximation error. However, the data processing script was written using the system simulation. Therefore, the coordinates system used in the script were not the same as the used by the calibration mechanical system. The mechanical calibration system had different axes rotations, so it was necessary to find a relation between the two systems. These two systems are shown in Figure 3.17.

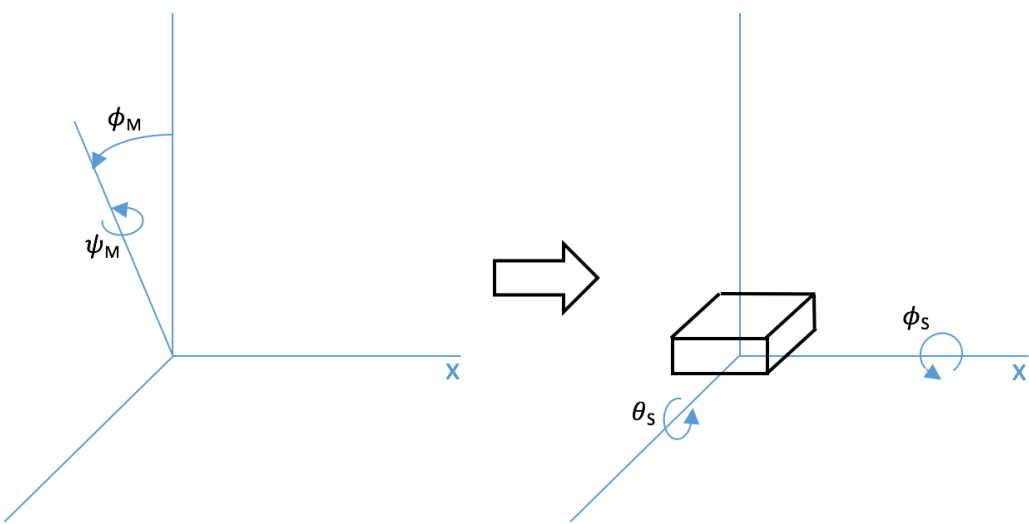


Figure 3.17 – Axes rotations for the calibration mechanical system (left) and the sensor light detection system (right)

Where the system in the left is the coordinates system that the calibration machine follows, and the system in the right is the photodiode light detection coordinates system.

To obtain this relation, the two systems were represented using Solidworks, and by using the smart dimensioning tool it was possible to modify both  $\phi_M$  and  $\psi_M$ . Therefore, this would automatically change both  $\theta_S$  and  $\phi_S$ , so it was possible to check if the relation found was correct. Therefore, with this 3D-sketch of the system the relation that was found is the one in Equation 3.5.

Therefore, after this was done, the Matlab script to perform this change was implemented, and the data in this base was saved in the sensor coordinates.

$$\phi_S = \arctan \left( \frac{\sin(\phi_M) \cdot \cos(\psi_M)}{\cos(\phi_M)} \right) \quad \text{and} \quad \theta_S = \arctan \left( \frac{\sin(\phi_M) \cdot \sin(\psi_M)}{\cos(\phi_M)} \right)$$

(3.5)

## 4. Results

### 4.1. Vacuum Test

One of the constraints of the system is that it must obviously be able to work in vacuum conditions. When the components were purchased all this was taken into account, and the range of temperatures of operation was also taken into account. However, with the photodiode, there was one problem. When it was purchased, there were only two options, the OPR5911 and the OPR5925. The main difference between these two components is that the OPR5911 has the cathodes of each photodiode bonded. However, the most significant difference, which is the reason why the OPR5911 was purchased, is that it has a higher effective area than the OPR5925, which would give a higher output current. However, none of them both were space qualified, and there was an annotation on both datasheets warning of applying pressure or high vacuum, as shown in Figure 4.1. This warning was worrying, since all the system must be vacuum resistant.

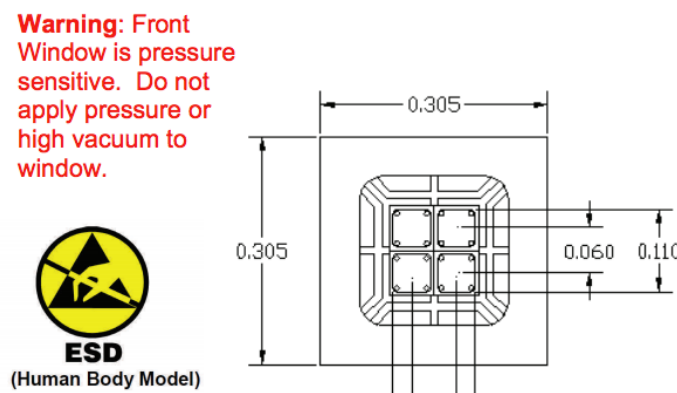


Figure 4.1 – OPR5911 High vacuum warning

However, since the textual specification of the datasheet was “Warning: Front Window is pressure sensitive. Do not apply pressure or high vacuum to window.” and the photodiode is intended to go to space the possibility that they had not really tested it in space conditions came up. This photodiode is used mostly for laser calibration or some similar applications, so it was possible that the manufacturer maybe had used its photodiode for one of these calibrations and they noticed that applying a pick and place sucker on the photodiode it broke. However, all of these were pure speculations so it was decided to design and test two systems applying to both of them the vacuum, with the TVAC provided in the lab, which can be seen in Figure 4.2.



Figure 4.2 – Thermal Vacuum Chamber

During this test, measurements were taken four times, once at the start, where there was normal pressure, once after 20 minutes after the start (with a pretty low pressure) and the last two, at the next morning, in high vacuum. Results are shown in Table 4.1, where PH1, PH2, PH3 and PH4 columns are the outputs of each photodiode.

Table 4.1 – Vacuum test results.

Pressure (mbar)	PH1	PH2	PH3	PH4	Illuminated
1000	43	43	43	43	Yes
52	43	43	43	43	Yes
$<10^{-5}$	43	43	43	43	Yes
$<10^{-5}$	1023	1023	1023	1023	No

It must be noted that the measurements were taken with an Arduino UNO board. This board ADC's have a 10-bit resolution, so it can represent a range from 0 to 1023. Therefore, since the output voltage of the circuit follows (3.1), when it is not being

illuminated the output voltage should be 3V, what after the AD conversion becomes a 1023.

Therefore, after checking the results, the conclusion was that the photodiode behaves correctly in the vacuum.

#### 4.2. Cover

As explained in section 3.2. of the thesis, the first idea was to create a glass-made reflective cover to achieve the required resolution. To do so, it was tried to perform the silver mirroring.

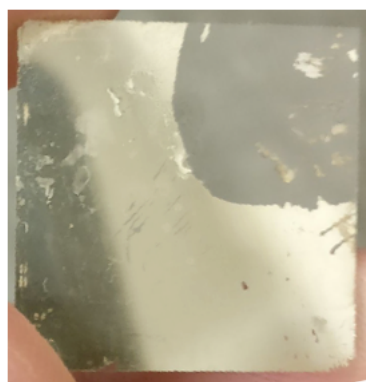


Figure 4.3 – Results of silver mirroring process in a coverslip

As it can be seen in Figure 4.3, the glass intended to silver mirror was a coverslip. This glass was compliant with the width requirement for the cover, and so the procedure was applied to it. After many attempts, the best result obtained is the one shown in the Figure 4.3. It was a good result because the mirrored area was larger than the photodiode size, so it was possible to cut it and apply the mirror design on it. However, the mirroring film was too thin and fragile, and by applying a little pressure it would go away. In addition, by looking at the glass from the other side, it was possible to see silver oxide, that had to be removed or be covered with something metallic in order to perform the attack to apply the cover design. This procedure was tried with sur-tin, a chemical tinning. The result was not successful, since the sur-tin did not snag on the oxide, but between the glass and the silver mirroring. Therefore, it was decided to go back to the film solution.

#### 4.3. Calibration Results

The calibration process was thought to be performed with Prof. Pablo Ortega's solar simulator. This is the finest simulator available in the university, so that's why it had been decided to be used. However, when the system was ready to be calibrated Prof. Pablo

Ortega's laboratory was under reconstruction, so the solar simulator was unavailable. That was a big problem, since all the mechanical system had been designed for that specific simulator.

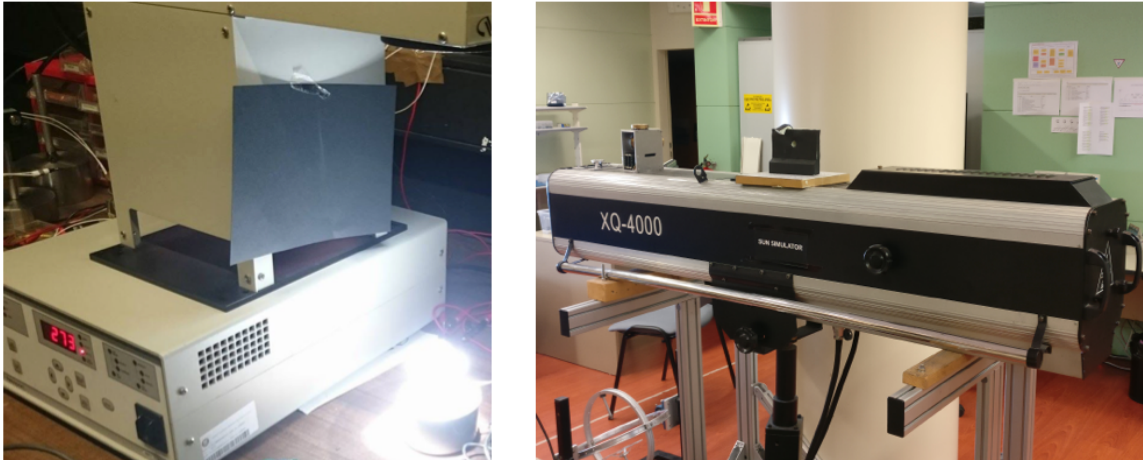


Figure 4.4 – Prof. Pablo Ortega's Sun simulator and NanoSat Lab's Sun simulator

Therefore, as it can be seen in Figure 4.4, where the solar simulator which the system had been designed for is the one in the left and the one finally used is the one in the right, these simulators do not have the same light direction. If the system was calibrated using the Oriel simulator, the calibration machine that had been made would have been the adequate, since the natural light direction for it is the upside coming direction. However, since finally it was necessary to use the one on the right-side in which the light is provided horizontally, the system designed could be adapted, but it was not the optimum to use. The first solution tried was to set the outside motor at 90 degrees, in order to have the light incident perpendicularly on the photodiode. However, when the motor had to do a 1-degree step, the weight of the inner platform was too high and it had not enough power to maintain this 1-degree steps. Then this solution was discarded, and the final one was implemented. It consisted to put the system in the position that can be observed in Figure 4.5.

To do so, the plates were cut in order to have the system leveled in this position too. This way, no motor was fighting directly against the gravity force, so theoretically it should have been easy to work. However, during the final calibration, the lamp of this simulator applied a higher heat than expected to the system, and the 3D printed piece dilated. The piece mainly dilated by the holes, the one for the screw and the bottom hole for the axis. After observing the movement of the 3D piece, it was noted that it was not rotating 360 degrees correctly. This problem was due to the tension applied by the connector cable. To solve these problems, a new 3D piece was made, which would be mainly the same,

but it would include two screw holes and two holes for nuts. This way, the piece would be correctly attached to the axis, and it would rotate correctly.

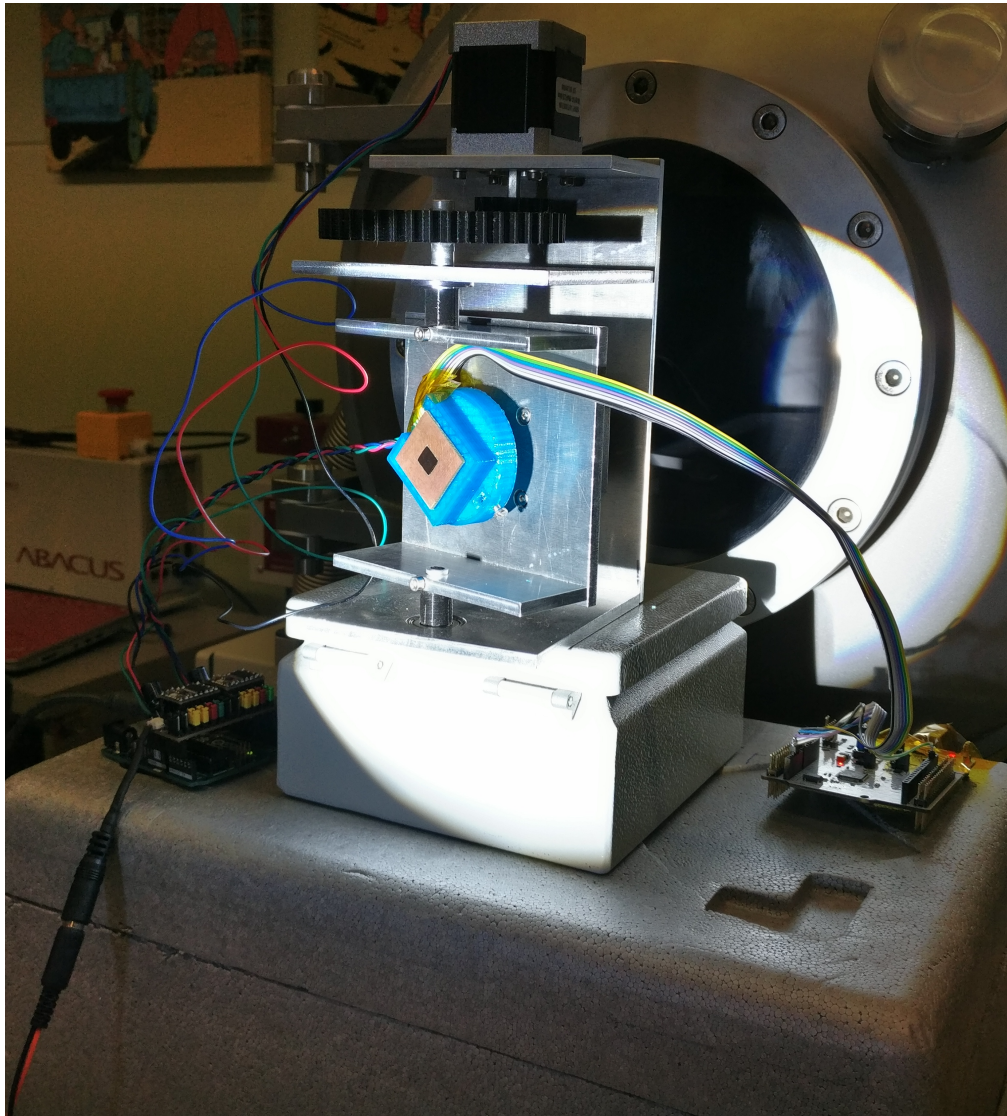


Figure 4.5 – Final Calibration system

After performing the calibration under the circumstances that have been previously commented, the results obtained are the following. The circuit output voltage follows Equation 3.1, but the STM performs an AD conversion. This means that the data stored in Matlab after the calibrations follows Equation 4.1.

$$ADC_{value} = (3 - R_f \cdot I_{ph}) \cdot \frac{4096}{3} \quad (4.1)$$

Analyzing the data, the minimum value found was 1883. Theoretically, the minimum should be 0, what would correspond to an output voltage of 3 volts of the circuit.

Therefore, by readjusting the feedback resistors, it was possible to obtain a larger resolution, obtaining a wider dynamic range between 0 and 4096.

However, this calibration data was loaded anyway to the Matlab estimation script, and the results were the following.

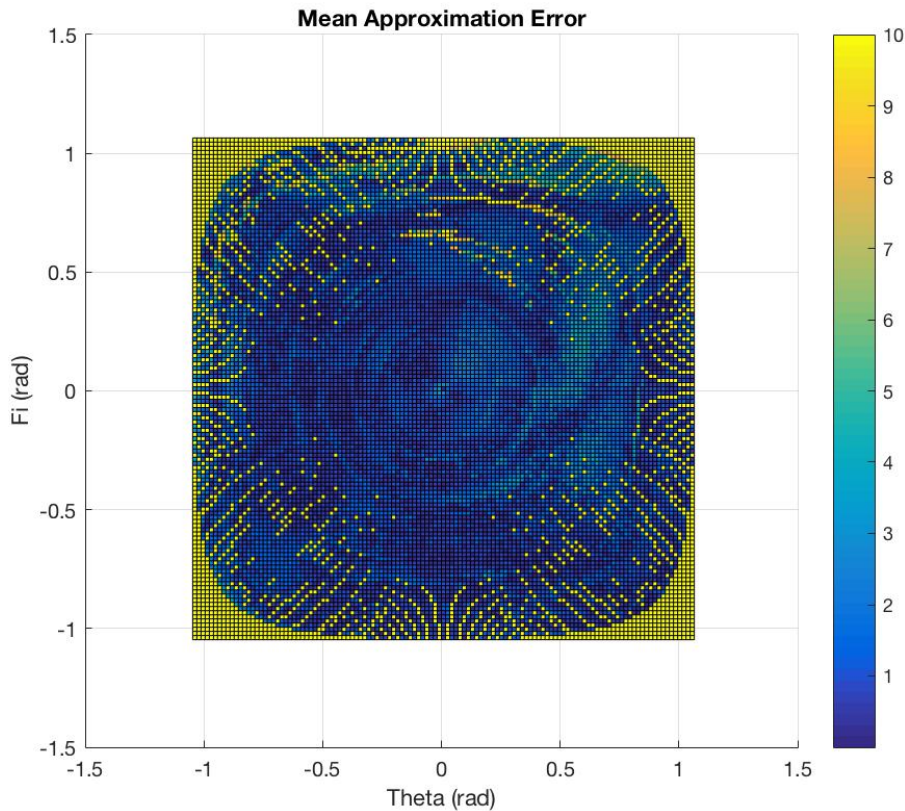


Figure 4.6 – Estimation error with real calibration data

Using a 9<sup>th</sup> order polynomial, the estimation performed was not compliant with the requirements. Both axes are the angles in radians, and the color represents the error. Dark blue is between 0 and 1 ° of error. Light blue is between 2 and 5 ° of error and finally yellow is an error higher than 7 °. Therefore, it can be seen, this is not a valid estimation, although, taking into account the fact that the ADC range is not used completely, so just changing the feedback resistor values and calibrating again, a better estimation could be performed, since in the center of the figure, the estimation is compliant with the requirements.

## 5. Budget

	Necessary	Minimum Quantity	Euros /u	Subtotal	Total
Quad op amp	5	5	3,75 €	18,75 €	
Connector	5	6	1,16 €	6,96 €	
Connector	5	5	0,31 €	1,54 €	
Resistance	40	40	0,01 €	0,58 €	
Regulator	5	5	5,78 €	28,90 €	
Capacitor	5	10	0,02 €	0,18 €	
Capacitor	5	10	0,07 €	0,68 €	
Capacitor	5	10	0,06 €	0,64 €	
Inductance	5	10	0,61 €	6,12 €	
Microcontroller	5	5	3,83 €	19,15 €	
Photodiode	5	5	5,50 €	27,50 €	
Ammonia	1	1	10,50 €	10,50 €	
Sodium Hydroxide	1	1	2,20 €	2,20 €	
Silver Nitrate	1	1	67,00 €	67,00 €	
Glycerin	1	1	10,95 €	10,95 €	
Slide cover	5	100	0,01 €	1,21 €	
PCB	5	10	1,29 €	12,90 €	
2.5 W Blue Laser	1	1	69,90 €	69,90 €	
Blue Laser Protection glasses	1	1	11,82 €	11,82 €	
Silicone elastometer KIT	1	1	186,69 €	186,69 €	
					<b>484,16 €</b>

	Credits	Hours by ECTS Credit	Hours	Price /Hour	Cost
Calibration Software implementation			50		400 €
Calibration Hardware design & test			80		640 €
I2C protocol design and implementation			180		1440 €
PCB Design, welding & Test			40		320 €
Glass cover manufacturing			60		480 €
Calibration process			60		480 €
Film cover attachment			20		160 €
Interpolation process design			30		240 €
System simulation			40		320 €
Vacuum Test			10		80 €
Full system testing			30		240 €
Illness			120		960 €
<b>Total</b>	<b>24</b>	<b>30</b>	<b>720</b>	<b>8 €</b>	<b>5760 €</b>

## **6. Conclusions and future development:**

In conclusion, it is possible to develop a low-cost Sun sensor with a good accuracy using the technique of covering part of the sensor, in order to obtain the desired accuracy. The results obtained are not compliant with the requirements, but with the changes proposed the performance will improve. The hardware for the sensor is not a problem in terms of cost, the main thing that will make the sensor price higher is the cover. The fact that the cover should be glass-made and reflective is not cheap, since the chemicals to perform the silver mirroring are not cheap, and the blue laser to cut the glass is also expensive. In addition, the system to fix the cover is also expensive, although it is previously purchased in other subsystems of the CubeSat.

As a future development, there is a lot to be done in the project. First of all, it is necessary to develop a good cover, since as has been explained in section 3.2, the solution that has been used to present this thesis is temporal. Therefore, a good silver mirroring performance can be done, or the sputtering machine solution may be considered. However, these are not the only options and maybe there is another better solution. It is important to point that not only is important to find a way to make the glass reflective, but also it is necessary to find a way to cut it. Glass cutter or blue laser are the two solutions proposed, although there may be better solutions. Anyway, the cover is a critical point that needs to be solved.

Another improvement that could be done, is the cover placing. Manually placing is not really a good option, since there will always be a large error. Although the calibration is thought to correct these errors, it would be better to avoid or reduce them from the beginning.

It is also necessary to improve the I2C program that will be running on the microcontroller. What has been done is a first version, which is functional and can be configured, but it is needed to perform a power consumption evaluation, taking into account the time in different working modes, in order to define the optimum clock frequency. Last but not least, it would be interesting to develop the possibility to send more data on the configuration call, what would imply the possibility to send to the microcontroller more than one byte I2C calls.

Finally, the last part that can be done is to design the whole system PCB. It has not been done in this thesis due to the fact that the solar panel PCB had not been designed yet. Therefore, once it is done, it is necessary to implement the PCB including everything, even the L053R8. However, this part should not be actually very difficult, since theoretically, all the bottom layer of the solar panel's PCB should be empty. Therefore, there is a lot of space to place the components and do the design.



As a recommendation for future development, a good idea would be to readjust first the feedback resistors, perform a new calibration and obtain a better estimation.

## **Bibliography:**

- [1] Swartwout, M. (2013). The first one hundred CubeSats: A statistical look. *Journal of Small Satellites*, 2(2), 213-233.
- [2] Heidt, H., Puig-Suari, J., Moore, A., Nakasuka, S., & Twiggs, R. (2000). CubeSat: A new generation of picosatellite for education and industry low-cost space experimentation.
- [3] Bester, J., Groenewald, B., & Wilkinson, R. (2012). Electrical power system for a 3U CubeSat nanosatellite incorporating peak power tracking with dual redundant control. *Przegląd Elektrotechniczny. Selected full texts*, 88, 300-304.
- [4] P. Via, 3Cat-4 Design Specification v1.0, March 2017
- [5] Joan A. Ruiz, 'Fly Your Satellite! 2017' CubeSat Proposal <sup>3</sup>CAT-4, March 2017
- [6] David A. Katz's Webpage. URL: <http://www.chymist.com/>
- [7] Hayashi, Fumio (2000). Econometrics. Princeton University Press. ISBN 0-691-01018-8.
- [8] Dismuke, C., & Lindrooth, R. (2006). Ordinary least squares. *Methods and Designs for Outcomes Research*, 93, 93-104.

## **Appendices:**

### **Appendix A: Work Plan Packages, milestones and Gantt Diagram**

#### **A.1. Work Breakdown Structure**

- Sun Sensor Design
  - o PCB Design
  - o PCB Welding
  - o Integration in whole CubeSat
  - o Glass cover manufacturing
  - o Cover attachment
- Calibration Process
  - o PCB Design
  - o PCB Welding
  - o Calibration Process Software
  - o Calibration Mechanical System
  - o Calibration Performance
- Software Development
  - o Base change
  - o Estimation Process
  - o I2C Communication Protocol

## A.2. Work Packages

Project: Sun Sensor Design	WP ref: 1	
Major constituent: Hardware Prototype	Sheet 1 of 3	
Short description: Design of the physical sensor. Includes the circuitry, the cover and the integration in the whole CubeSat.	Planned start date: 15 <sup>th</sup> February 2017 Planned end date: 25 <sup>th</sup> May 2017	Start event: Design of the PCB End event: Cover Placing and attachment
Internal task T1: Design of the PCB. Internal task T2: PCB Welding. Internal task T3: Integration in the whole CubeSat. Internal task T4: Glass cover manufacturing. Internal task T5: Cover placing and attachment.	Deliverables: Degree Thesis	Dates: 30 <sup>th</sup> June 2017

Project: Calibration Process	WP ref: 2	
Major constituent: Simulation	Sheet 2 of 3	
Short description: Design of both the hardware and the software necessary to calibrate the sensor.	Planned start date: 15 <sup>th</sup> February 2017 Planned end date: 30 <sup>th</sup> June 2017	Start event: Software to store data received by the microcontroller End event: Perform the calibration
Internal task T1: Design a PCB to control the stepper motors Internal task T2: Weld the PCB to control the stepper motors Internal task T3: Design software to store the data received by the sensor microcontroller. Internal task T4: Adapt the mechanical system to the Sun simulator. Internal task T5 (To be done once WP1 ended): Perform the calibration	Deliverables: Degree Thesis	Dates: 30 <sup>th</sup> June 2017



Project: Software Development	WP ref: 3	
Major constituent: Simulation	Sheet 3 of 3	
Short description: Develop software to estimate the sunlight direction. Design and implement an I2C protocol to communicate with the OBC.	Planned start date: 20 <sup>th</sup> March 2017 Planned end date: 6 <sup>th</sup> June 2017	Start event: Estimation Process End event: Base change
Internal task T1: Design an estimation process since all the calibration data can't be loaded to the microcontroller Internal task T2: Design and implement an I2C protocol to communicate with the OBC. The system shall be configurable and must use low-power consumption modes of operation. Internal task T3: Perform the base change script.	Deliverables: Degree Thesis	Dates: 30 <sup>th</sup> June 2017

### A.3. Milestones

WP#	Task#	Short title	Milestone / deliverable	Date (week)
1	1	PCB Design (Sun Sensors)		24/02/2017
1	2	PCB Welding (Sun Sensors)		09/03/2017
1	3	Integration in whole CubeSat		17/03/2017
1	4	Glass cover manufacturing		17/05/2017
1	5	Cover placing and attachment		25/05/2017
2	1	PCB Design (Motors Control)		08/03/2017
2	2	PCB Welding (Motors)		14/03/2017
2	3	Calibration Software		01/03/2017
2	4	Adapting mechanical system		23/06/2017
2	5	Calibration of the System		30/06/2017
3	1	Estimation Process		27/03/2017
3	2	I2C protocol design and implementation		01/06/2017
3	3	Base Change		07/06/2017

#### A.4. Gantt Diagram

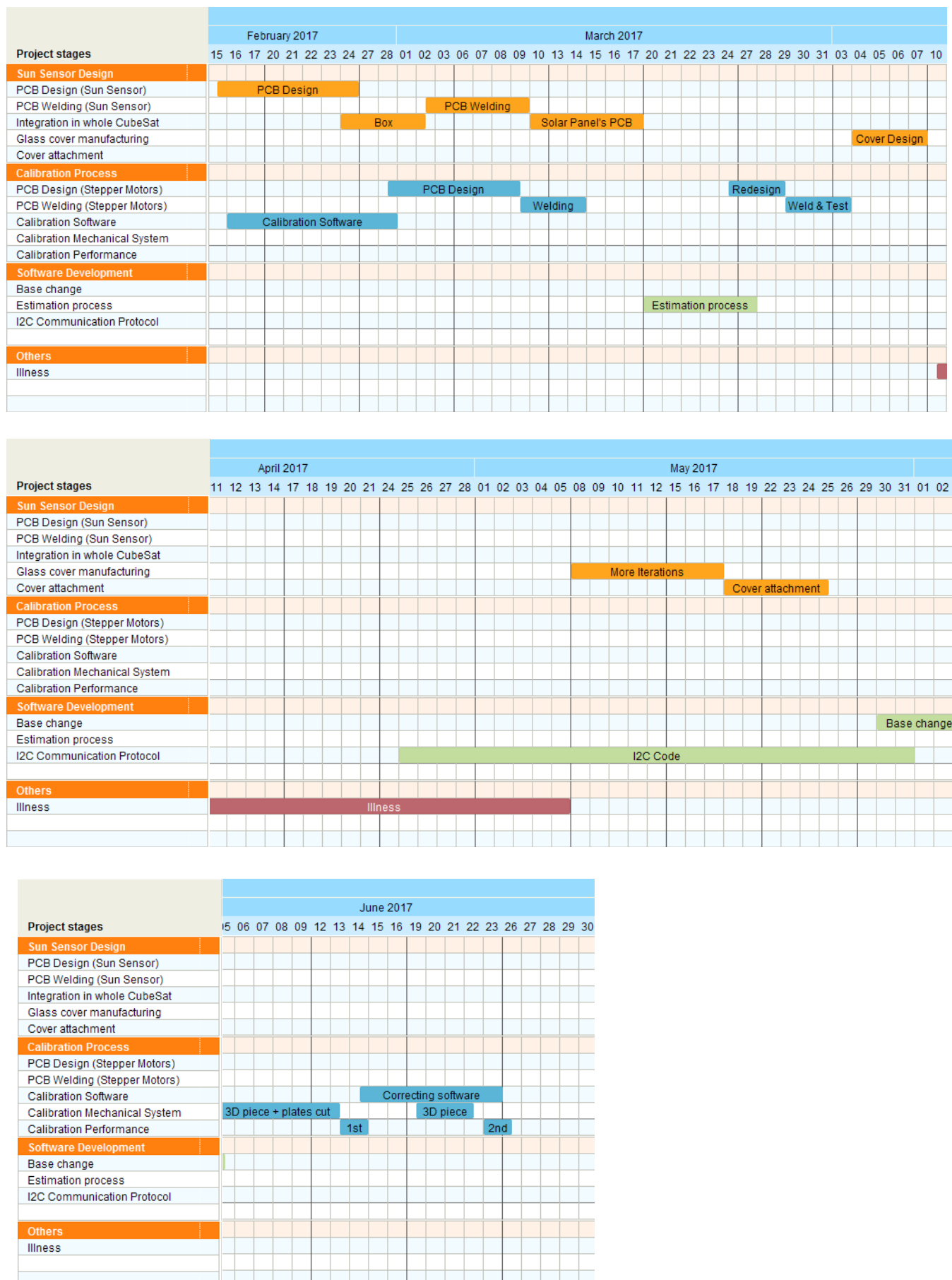


Figure A.1 – Gantt Diagram

## Appendix B: Matlab system simulation

In order to simulate this system, the software used is Matlab. First of all, it was necessary to decide which would be the cover design that would be applied. After looking to the products that satisfy these needs in the actual market, it was decided to try to implement a window that had an aperture in the middle, and in order to give it more resolution, it was decided to add to it a cross. To simulate and test this idea, it was necessary to implement a real-dimension model of the 2x2 photodiode array, covered with the window designed. Although other possibilities such a cover with only a circular aperture were considered this cover design was simulated and was compliant with the requirements. Another good point of this design is that the fact that it had no circular drawings would make the placing easier, since manual placing would depend a lot on the possible references, and having straight lines would create easier references.

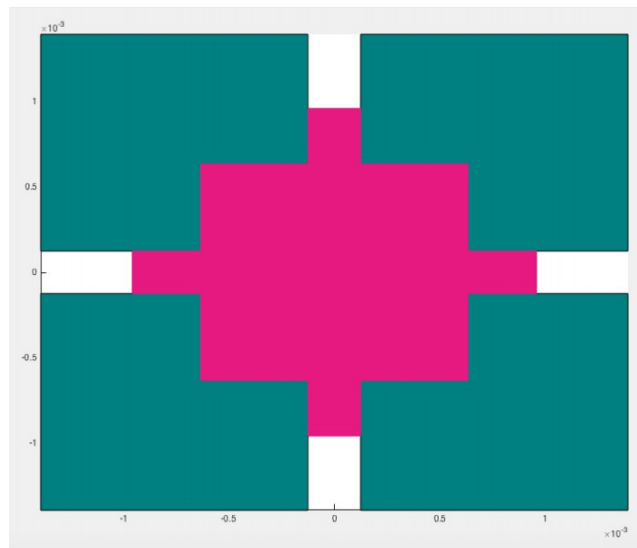


Figure B.1 – Top view of the system simulated

This idea can be seen in Figure B.1, where the green squares are photodiodes, and the pink part is the part of the cover that would be transparent, what means, the part through which the light would incise.

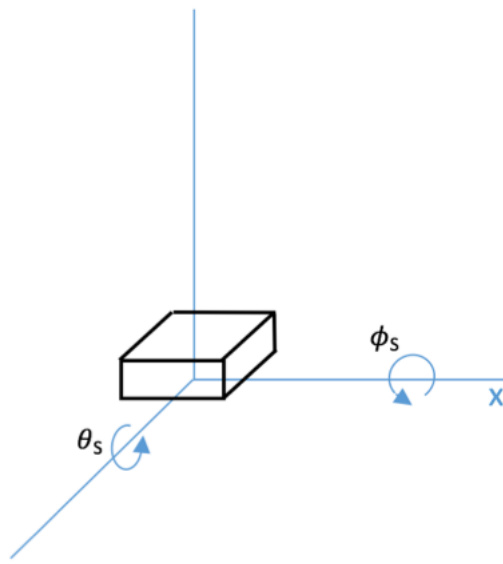


Figure B.2 - Angles used in the simulation

These simulations were performed using the  $\phi_s$  and  $\theta_s$  angles shown in Figure B.2. These angles represent the rotation in the two axes. After running the Matlab script that would simulate the illumination for each angle, the illuminated area for each photodiode is the one shown in Figure B.3. In this figure, each one of the peaks corresponds to one photodiode, so as can be seen the 4 photodiodes illuminated area are overlapped in this figure.

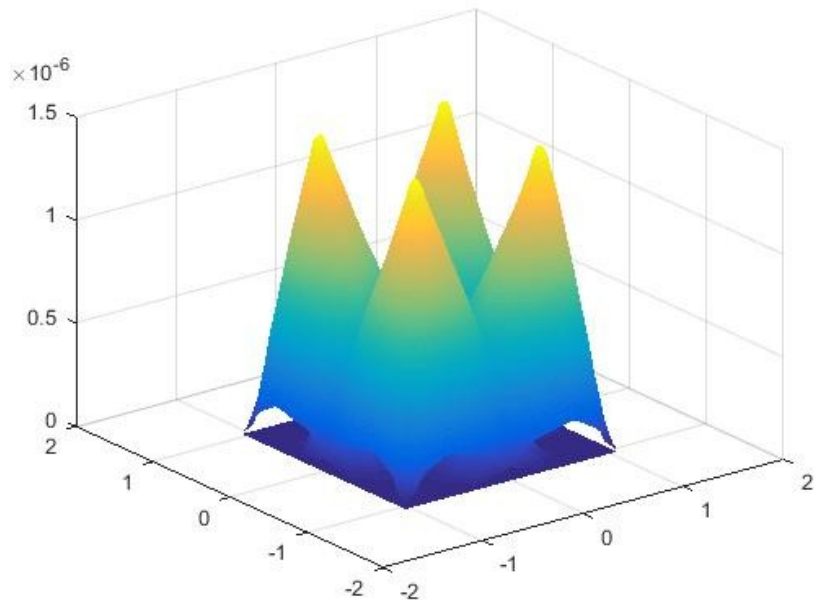
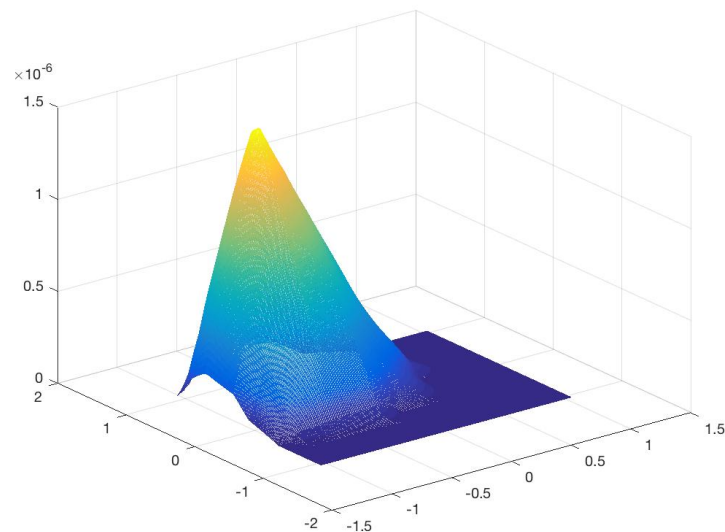
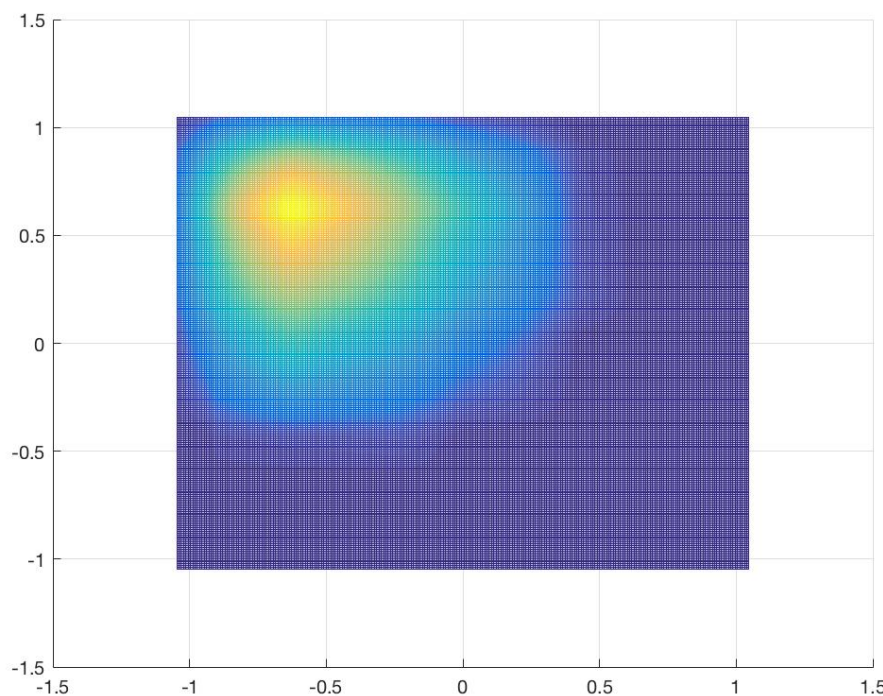


Figure B.3 – Illuminated area of each photodiode for each of the possible angles

As it can be seen in Figure B.4.a and Figure B.4.b, if only one photodiode's illuminated area is plotted the curve shape can be seen much better, without the other photodiodes information covering. As it can be observed, this curve has many points with the same size of the area illuminated so, in order to be able to determine the light direction, it is necessary to use information from all four photodiodes.



a)



b)

Figure B.4 – Illuminated area of one photodiode

Once the illuminated area of every single photodiode for each angle with the real-dimension model designed was obtained, the output current of each photodiode was obtained, for every possible angle too.

To do so, since the output current follows:

$$I_{out}(\theta_S, \phi_S) = \text{Area}_{ILL} \cdot \int \text{SpectResp}(\lambda) \cdot \text{Irr}(\lambda) \cdot d\lambda \quad (\text{B.1})$$

where  $\text{Area}_{ILL}$  is the illuminated area for a specific  $\theta_S$  and  $\phi_S$ ,  $\text{SpectResp}$  is the spectral responsivity of the OPR5911, given in the datasheet,  $\text{Irr}$  is the extraterrestrial Sun spectrum, and  $\lambda$  is the wavelength. Therefore, having downloaded the extraterrestrial solar spectrum the spectral responsivity was linearly interpolated in order to have the same number of samples and then integrated using the trapz function of Matlab. Then the results obtained were multiplied by 0.45, which was the maximum responsivity value, since the graphic given in the datasheet was the normalized one as seen in Figure B.5.

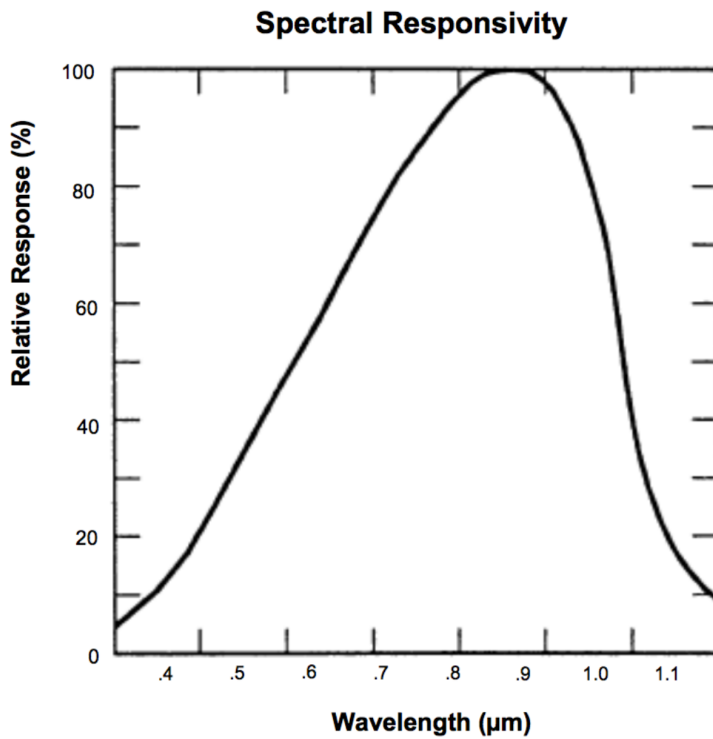


Figure B.5 – Spectral Responsivity of the OPR5911

Once this point is achieved, it is only necessary to take into account the directional sensitivity, in order to have as an output the current for each photodiode. To do so, the directional sensitivity is approximated by a cosine in one dimension. However, since the photodiode is sensible in two dimension, it is finally approximated by:

$$\text{DirSens} = \cos(\sqrt{\tan^2(\theta) + \tan^2(\phi)}) \quad (\text{B.2})$$

Therefore, by multiplying both Equation B.1 by Equation B.2 it is possible to obtain the output current for a specific  $\theta_s$  and  $\phi_s$ . The result is shown in Figure B.6, where the output current for each photodiode in every possible sunlight direction is shown.

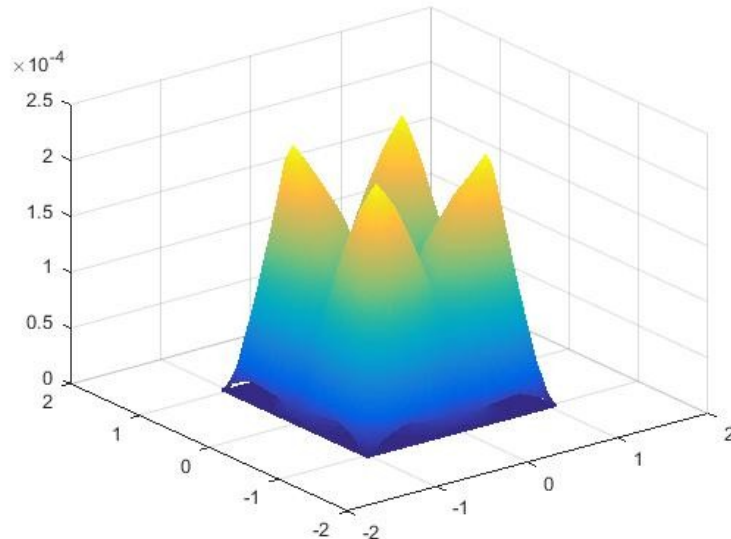


Figure B.6 - Output current for each photodiode for all the possible angles

Using these data, the theoretical maximum output current of the photodiode can be computed. Therefore, since the output voltage of the circuit depends on the current flowing from the photodiode, the feedback resistor value was chosen according to this value of current. However, the final range was not the expected, and it was due to the fact that the output current was not so high, so a possibility is to adapt the system to the real maximum output value of the photodiode current.

## Appendix C: Circuit Design

### C.1. Photodiodes: OPR5911 and OPR5925

Both models are Surface Mount Quad Photodiodes enclosed in a polyimide chip carrier and designed for control applications. In the case of the OPR5911 all cathodes are bonded together while in the OPR5925 case each cathode and anode is bonded separately. Both elements are designed to work in an operating range of temperatures from -55 °C to 125 °C. The fact that the OPR5911 model does not have 4 independent cathodes is not really a problem, since all of them will be short-circuited anyway. OPR5911 is the one being used, since it has a larger effective area, what will give a higher maximum output current, and therefore, a higher range of output current to determine the Sun position.

Table C.1 – Electrical characteristics extracted of the OPR5911

Electrical Characteristics ( $T_A = 25^\circ C$ unless otherwise noted)						
SYMBOL	PARAMETER	MIN	TYP	MAX	UNITS	TEST CONDITIONS
R	Responsivity	.45	-	-	A/W	$E_e = 10 \mu W, \lambda = 890 nm, V = 0 V$
$V_{BR}$	Reverse Breakdown Voltage	35	-	-	V	$I_R = 100 \mu A$
$I_D$	Reverse Dark Current	-	-	30	nA	$V_R = 10 V$
$C_T$	Capacitance	-	10	-	pf	$V_R = 10 V$
LxW	Active Area (per diode)	-	0.75	-	mm <sup>2</sup>	(0.86 mm x 0.86 mm)

Notes:  
(1) Solder time less than 5 seconds at temperature extreme.

The above table shows the electrical characteristics of the OPR5925 model in standard conditions (25 °C). The responsivity measures the electrical output per optical input at the wavelength  $\lambda=890$  nm. Since the Sunlight is composed by all wavelengths, it is going to be required to integrate the Spectral Responsivity of the photodiode. Reverse Breakdown Voltage (the amount of reverse bias that will cause the diode to break down and conduct in the reverse direction) is not needed to be considered since the electronic circuit works in photovoltaic mode (zero biased) and it is unlikely to breakdown. Reverse Dark Current (leakage current that flows when a bias voltage is applied to a photodiode) is almost negligible due to the fact that no bias voltage is applied. The last data depicted is the Active Area which transforms the incident light into electric intensity. The smaller it is the smaller the Capacitance is going to be and it will allow a higher signal-to-noise ratio.

The photodiode equivalent circuit is depicted in the next figure:

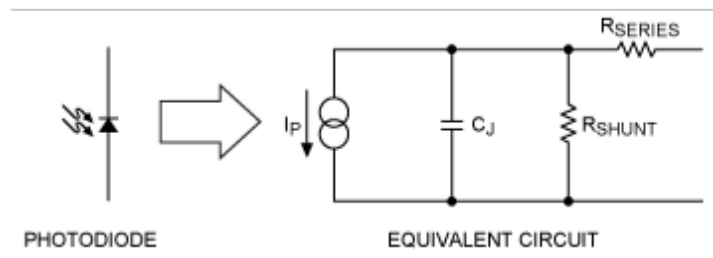


Figure C.1 - Equivalent circuit of a photodiode

$R_{SERIES}$  can be omitted due to its low value (the resistance produced by the wires and other mechanical parts).  $R_{SHUNT}$  (resistance of the zero-biased photodiode junction) needs to be considered but its value is not provided by the manufacturer, it has been considered to be a value of around  $100 \text{ M}\Omega$ . The theoretical maximum Intensity is going to be produced in one photodiode is  $222 \mu\text{A}$ .

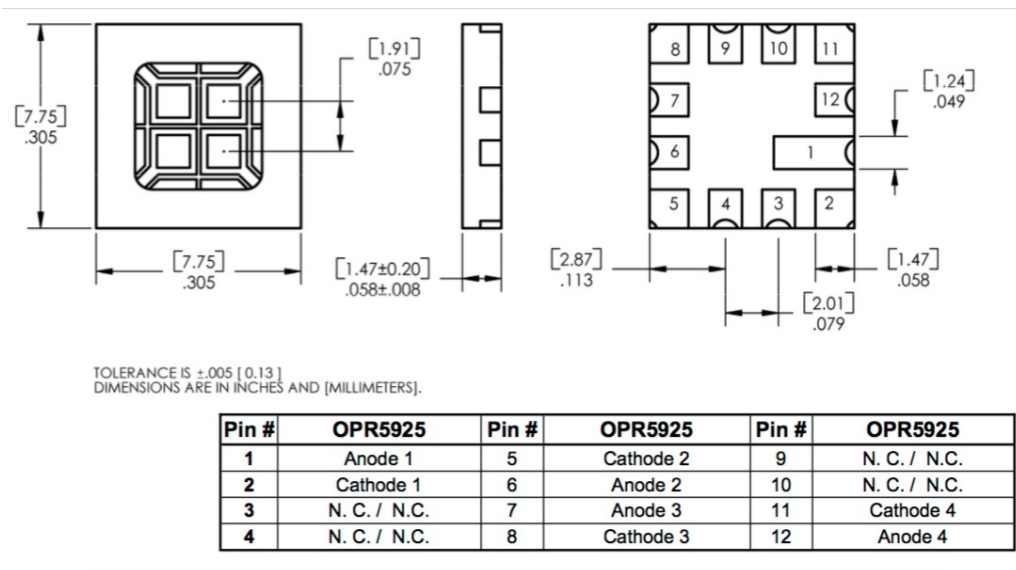


Figure C.2 – Pin configuration and physical dimensions of the OPR5925 model

## C.2. Voltage Regulator: LT6654-3

The LT6654-3 is a small precision voltage reference that offers high accuracy, low noise, low drift, low dropout and low power. Its temperature range values are fully specified from  $-55^\circ\text{C}$  to  $125^\circ\text{C}$ . The model chosen is the 3V output voltage and it is encapsulated in 6-lead SOT-23 package. Pin configuration and the recommended connection are shown in Figure C.3:

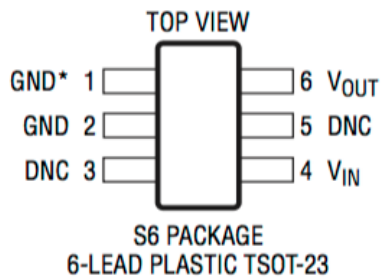


Figure C.3 – Top view of the pin configuration for the S6 package model

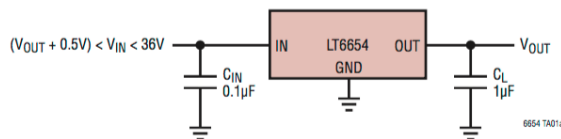


Figure C.4 – Recommended configuration of the LT6654

### C.3. Quad Operational Amplifier: LT6005HGN

A Rail-to-Rail input and output operational amplifier designed for portable applications. This amplifier operates on supplies that can be from 1.6V to 16V, in the Sun sensor system, it will be supplied with 3V and ground. The specified range of temperatures of the device goes from -40 °C to 125 °C, which fits perfectly with space conditions. The package chosen is a GN Package 16-Lead Plastic SSOP that is a quad (4 AO's in one package) type. Figure C.5 shows the pin configuration:

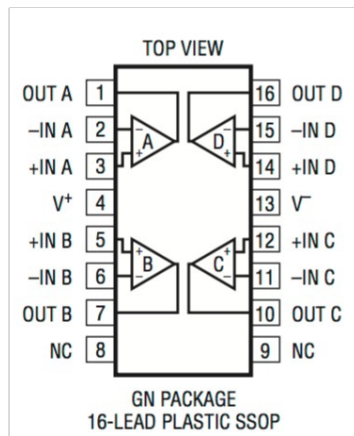


Figure C.5 – Physical connections of the GN Package 16-Lead, with the 4 AO's sharing the V+ and V- supplies.

Moreover, other characteristics to take into account are its Low Input Bias Current (90 pA maximum), its Low Input Offset Voltage (500 µV maximum) and its Low Input Offset Voltage Drift (2 µV/oC).

#### C.4. Filter

The filter in the output of the LT6654 has the following components.

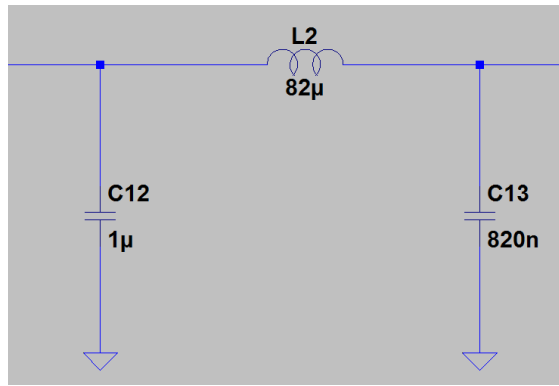


Figure C.6 – Filter design

The capacitor in parallel of 1  $\mu$ F is the one recommended by the LT6654 manufacturer and the inductance and capacitor in the right form a second order Low Pass Filter with cutoff frequency around 20 kHz. This filter has been designed to avoid possible interfering signals coming from other subsystems of the CubeSat that work at a higher frequency.

#### C.5. Transimpedance Gain Amplifier Design

A photodiode can be operated in one of two following modes: photoconductive (reverse bias) or photovoltaic (zero-bias). The photovoltaic mode reduces the response time because the additional reverse bias increases the width of the depletion layer, which decreases the junction's capacitance. Although this mode is faster, the photoconductive mode tends to exhibit more electronic noise. After looking information for the pros and cons of each design, it was concluded that the time response of the photovoltaic mode was compliant with the system requirements, and with this option it was possible to get a higher accuracy in the results.

The circuit would be supplied directly from the output of the voltage reference (3V) to the photodiode and the two typical resistances of any transimpedance scheme will allow to modify the output. Considering the ideal scenario where no current enters the AO inputs, the output voltage will be:

$$V_{out} = 3 - R_f \cdot I_{ph} \quad (C.1)$$

In no light conditions the intensity in the photodiode would be 0 and the output voltage would be equal to the supply one, and with maximum light it would be desired to get 0 V as output to get the full 3 V as range of possible values. Once this has been said, all the data acquired from the simulations in Matlab was analyzed and then deduced the maximum intensity the photodiode would produce, so isolating the  $R_F$  and with 0V as an

output in maximum light conditions it was found that the closest standard value of resistance for this system purpose would be 13.3 K $\Omega$ .

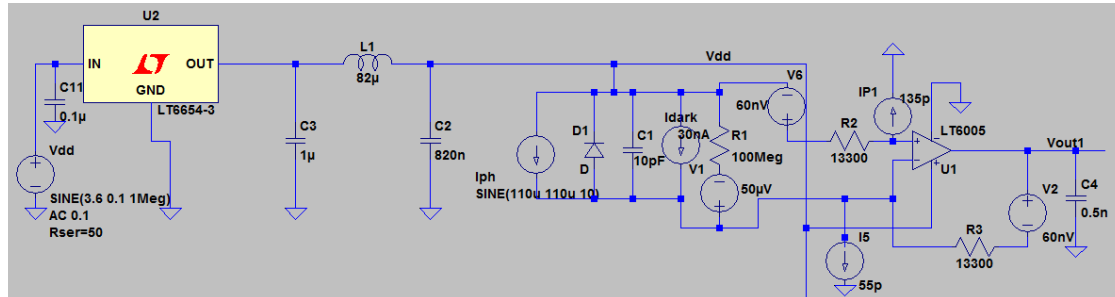


Figure C.7 – Schematic of the circuit for each photodiode

The schematic has a sinusoidal source of 1 MHz simulating some imperfections from the source. It also can be seen the equivalent circuit of the photodiode and a capacitance (C4) in the right corner. It has been added for stability reasons and 500 pF is the maximum capacitive load handling by the LT6005HGN operational amplifier.

All the components in the circuit (resistors, capacitors and inductances) used are SMD (Surface-Mount Device). The temperature range of the resistors goes from -55 °C to +125 °C, the inductance range goes from -20 °C to +85 °C, and the capacitor temperature range goes from -55 °C to 105 °C.

To simulate the light conditions that the nanosatellite will face in open space,  $I_{PH}$  has been modified with a DC intensity (the average  $\sim 110 \mu\text{A}$ ) and an amplitude of the same value (obtaining a range of 0 to 220  $\mu\text{A}$ ) with a frequency of 10 Hz.

## Appendix D: Circuit simulation

Incident light on the photodiode will provide an output current for each own photodiode of the 2x2 array. Therefore, the goal of the system is to obtain the information given these currents. In order to do that the system will have voltage inputs into the ADC's so a circuit that converted from current to voltage was designed. This circuit was also simulated, by using the LTSpice software. This software has the features of running the circuit in both temporal and frequency domains.

Once it was simulated, it was proven that it was compliant with the system. Then errors were added, in order to have a more realistic simulation. The errors that were taken into account were component errors such as the  $I_{bias}$ ,  $V_{offset}$  and value fluctuations due to temperature or tolerance of the components. The first two were obtained directly from the functions (relation between  $I_{bias}$  and  $V_{offset}$  with the temperature) provided by the manufacturer. The fluctuations due to the temperature were simulated adding a voltage source in every resistance of value equal to the resistor thermal noise formula:

$$e_{out} = \sqrt{4 \cdot K \cdot T \cdot B \cdot R} \quad (D.1)$$

where  $k = 1.38 \cdot 10^{-23}$  J/K is the Boltzmann constant,  $T$  is the Temperature in Kelvin,  $B$  is the noise Bandwidth in Hz, and  $R$  is the Resistor value in ohms. Therefore, the error produced by the components of the circuit and their imperfections was obtained and computed too.

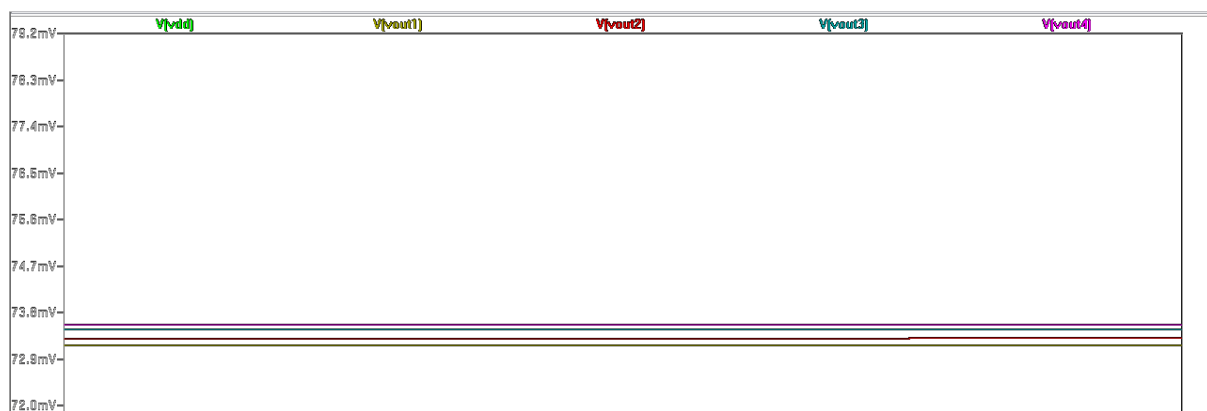


Figure D.1 - Output voltage difference due to temperature variations

Temperature values in Figure D.1 are: -25 °C, 25 °C, 80 °C and 120 °C. Temperature causes changes in  $I_{BIAS}$ ,  $V_{OFFSET}$ ,  $R$  and so on.

The LT6654-3, is a low noise precision voltage reference which gives a 3V output voltage reference. It was necessary to filter this signal of reference, since it could have interference coming from the source but also coming from the magnetorquers circuit.

After studying the frequencies that could interfere it was specified to try to get a second-order filter of 10 or 1 kHz. After many designs, the filter designed is the one shown in Figure D.2, also show in Appendix C CIRCUIT, which as can be seen in Figure D.3 and Figure D.4, behaves correctly in both temporal and frequency domains.

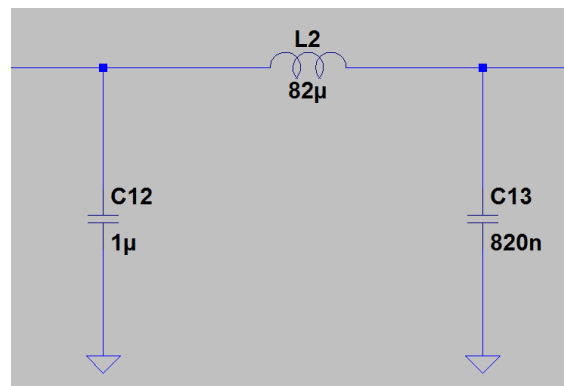


Figure D.2. – Final design of the filter including the  $1\mu\text{F}$  capacitor

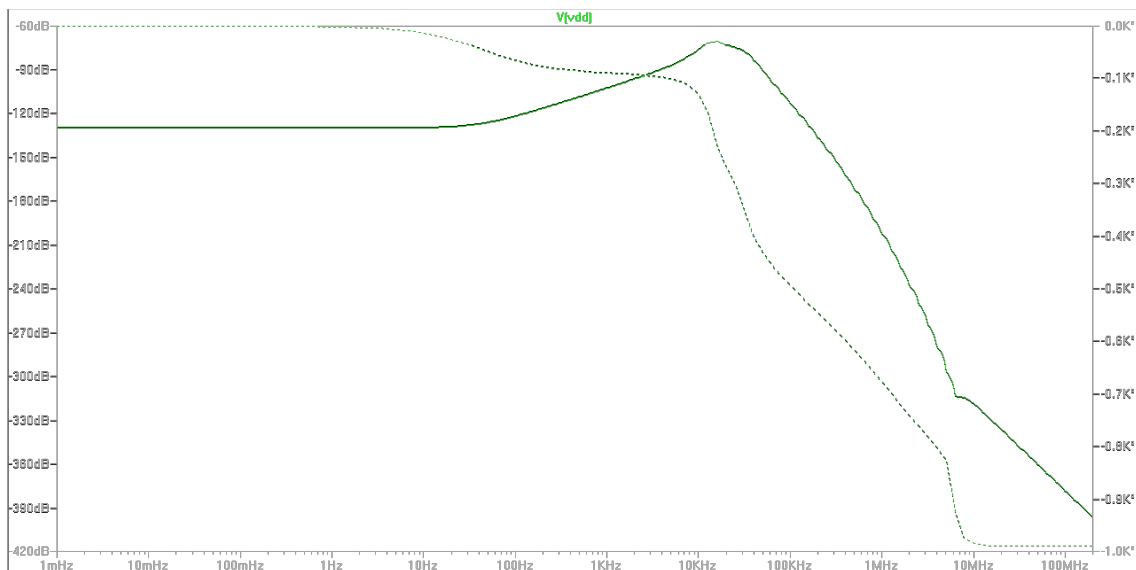


Figure D.3 – Filter response in frequency domain.

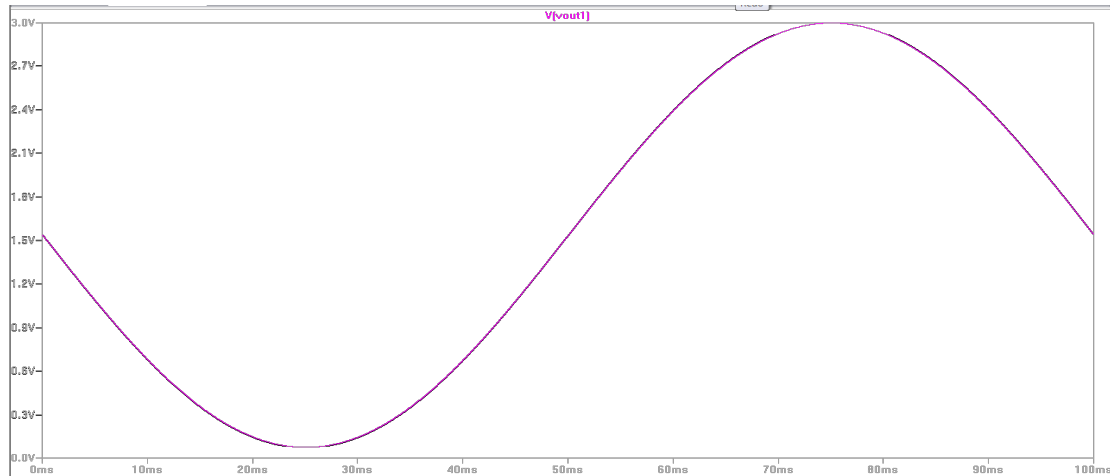


Figure D.4 – Filter response in temporal domain

Some previous designs had a better frequency response, but had other bad points, such as power consumption or bad performance in the temporal domain. An example is shown in Figure D.5.

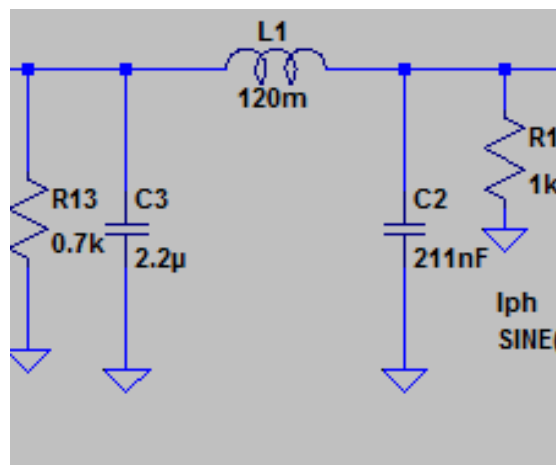


Figure D.5 – First design with the resistors in parallel

The resistors were placed to avoid oscillations in temporal domain. It worked correctly, but the inductance takes a value of 120 mH, not a typical value. This filter behaved correctly and had a cutoff frequency of 1 KHz, but it had a higher power consumption due to the parallel resistors.

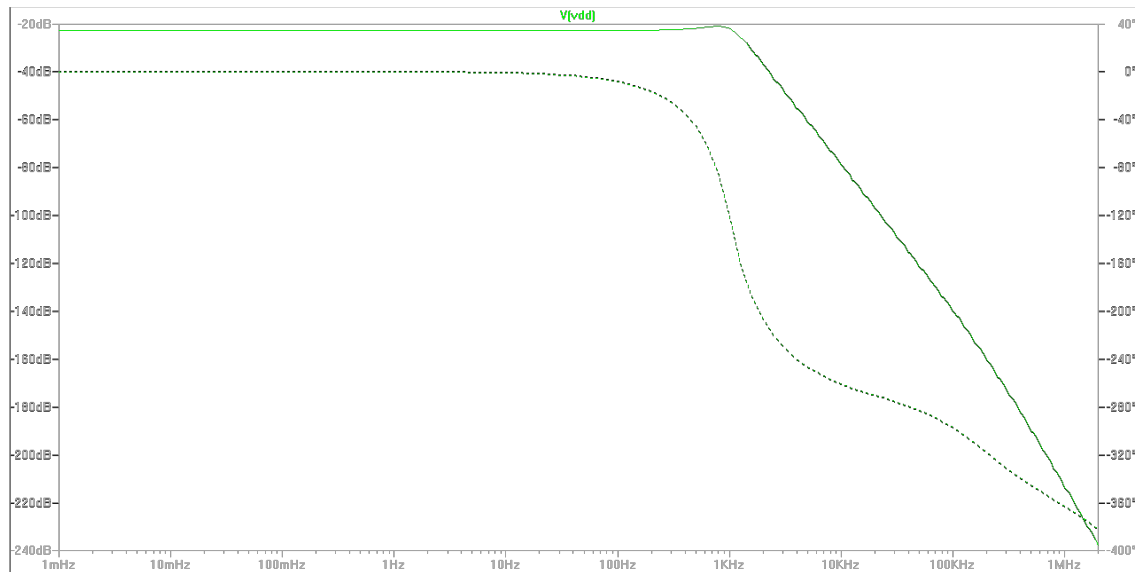


Figure D.6 – Filter response in frequency domain

## Appendix E: Estimation Process

The estimation script has three main parts. First of all, it will read the data for each photodiode stored in an Excel sheet. This sheet should have the output voltage value for each angle, for the four photodiodes. The next step of this script is to calculate the polynomial length, given a specific order. Once the length has been computed, it is necessary to compute the matrix  $X$ , and transpose it. Finally, it is just necessary to perform the following operation.

$$H = (X^T \cdot X)^{-1} \cdot X^T \quad (\text{E.1})$$

The obtained matrix is  $H$ , which multiplied by the sample vector will give the coefficient arrays for both,  $\phi_s$  and  $\theta_s$ . These two arrays are the ones to be loaded in the microcontroller's memory in order to perform the estimation.

These calculations are performed according to the OLS estimation. The Sum of Squared Residuals (SSR) follows:

$$S(b) = \sum_{i=1}^n (y_i - x_i^T \cdot b)^2 = (y - X \cdot b)^T \cdot (y - X \cdot b) \quad (\text{E.2})$$

The idea is to find the value of  $b$  that minimizes the sum, which is called the OLS estimator:

$$\hat{\beta} = \underset{b \in \mathbb{R}^p}{\operatorname{argmin}} S(b) = \left( \frac{1}{n} \cdot \sum_{i=1}^n x_i \cdot x_i^T \right)^{-1} \cdot \frac{1}{n} \sum_{i=1}^n x_i \cdot y_i = (X^T \cdot X)^{-1} \cdot X^T \cdot y \quad (\text{E.3})$$

After the parameter  $\beta$  has been estimated, the predicted values follow Equation E.4.  $\hat{\beta}$  in E.4 is the  $\phi_s$  coefficient array or the  $\theta_s$  coefficient array in the Sun sensor estimation script.

$$\hat{y} = X \cdot \hat{\beta} = P \cdot y \quad (\text{E.4})$$

In order to perform the final estimation, it is necessary to perform the polynomial approximation. To do so, those polynomial values which are function of the diode output are computed and later on multiplied first of all by the alpha estimation vector and after that the same polynomial values vector is multiplied by the beta estimation vector. With these two multiplications the result obtained are two numbers, which are the estimated  $\phi_s$  and  $\theta_s$ .

Once these two estimations have been performed for each angle, since the Matlab script first task was to read the output data of the sensors (simulated), it is possible to compare



the estimation with the simulated data, in order to compute the estimation error. Then, by getting the absolute value of the difference between alpha output matrix and alpha estimation matrix, it is possible to obtain the error in alpha. The same must be done to obtain the error in beta. To compute the general error, the only thing that has to be done is to compute for each angle:

$$\sigma^2(\phi_s, \theta_s) = \sigma_\phi^2 + \sigma_\theta^2 \quad (\text{E.5})$$

## Appendix F: Calibration process

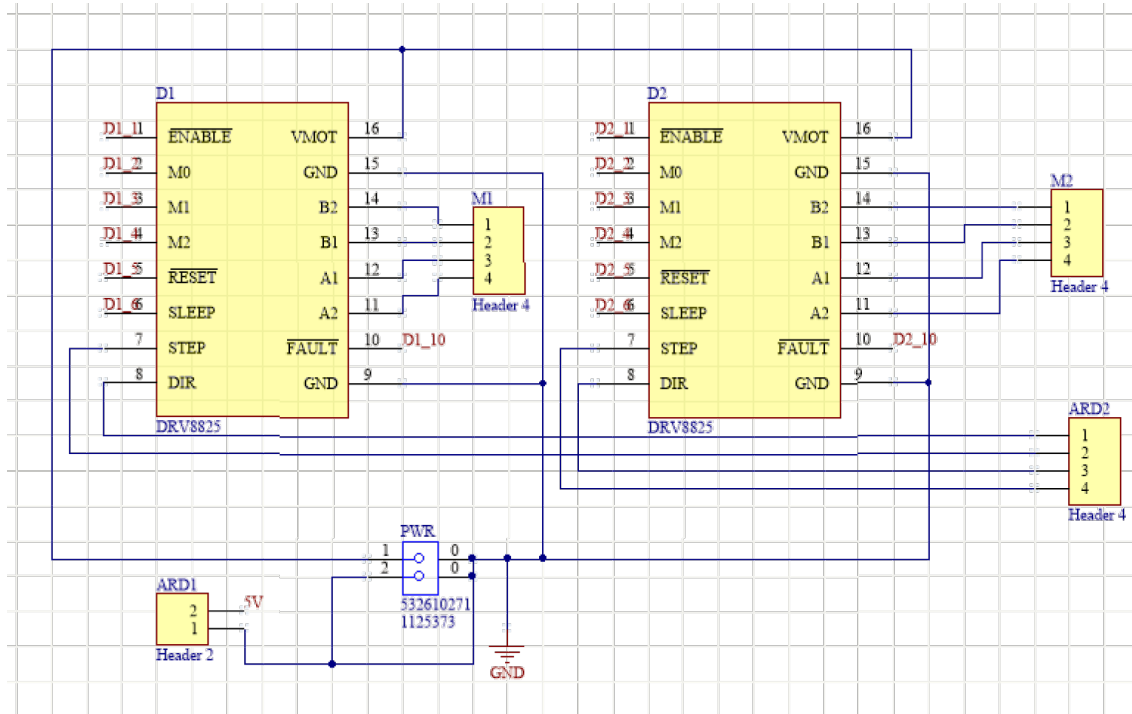


Figure F.1 – Schematic of the drivers' circuit

Figure F.1 shows the schematic of the PCB that controls the motors for the calibration. This circuit, has two main components, two drivers, D1 and D2 in the picture. As can be seen, each driver has a four output connection, M1 and M2. These connectors are the ones that connect the driver to the motor, in order to control them. With the Arduino UNO board, the step and direction of each motor will be controlled, that is why there is another header (ARD2), which will control the step and direction for each motor individually. Finally, there is the last header, ARD1, which will be used to take 5V and GND. Last but not least, the Molex two-pad connector can be found, which is used to take the power supply of the motors.

In order to attach the PCB to the calibration machine, a 3D model piece was designed. The 3D representation can be found in Figure F.2.

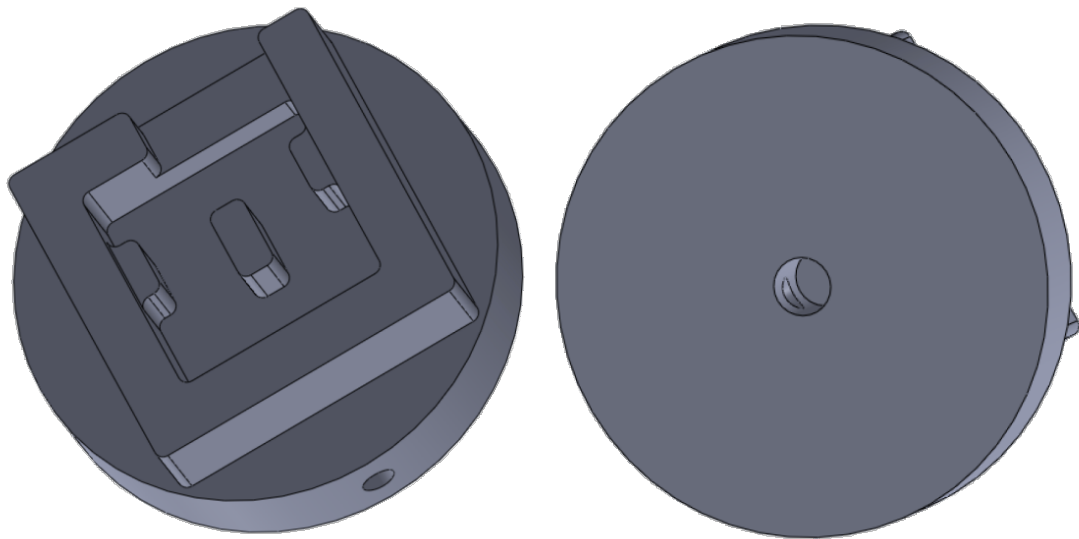


Figure F.2 – Piece used to attach the PCB to the calibration machine

As shown, the piece has two main parts the base and the PCB container part, which is circular and has a hole in the bottom and in the lateral face. The hole in the bottom is to make the axis of the motor enter, and the one in the lateral face is to put a M3 screw to attach the piece to the axis. The square aperture in the middle is to contain the PCB, and it has the same dimensions as the PCB, so that the PCB does not move. In order to have the PCB leveled, the three columns have been positioned specially where the PCB does not have any component. Finally, the square containing the PCB, has an aperture to connect the PCB with the microcontroller board. Final result of the piece integrated in the calibration system can be found in Figure F.3.

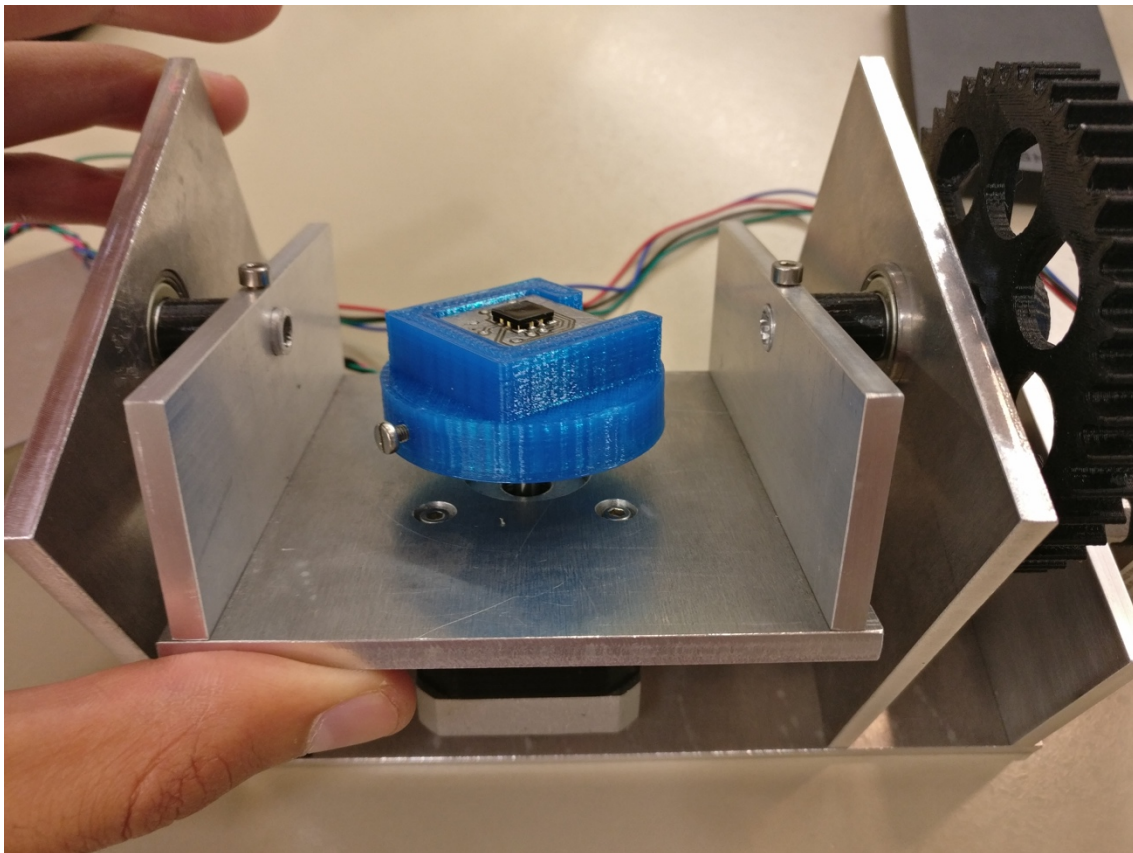


Figure F.3 – First 3D piece attached to the calibration machine

As commented in the calibration results section of the thesis, this system had two main inconveniences. First of all, the heat coming from the lamp would dilate the piece, what would make the holes wider. Obviously, as a consequence of this, the screw would not press correctly the piece to the axis and, since the axis hole had also widened, the piece would not rotate correctly. In order to solve this, since the heat would be applied anyway, it was interesting to find a solution strong enough to support the cable tension. The solution to these problems is the one commented in the calibration, and its design is shown in Figure F.4.

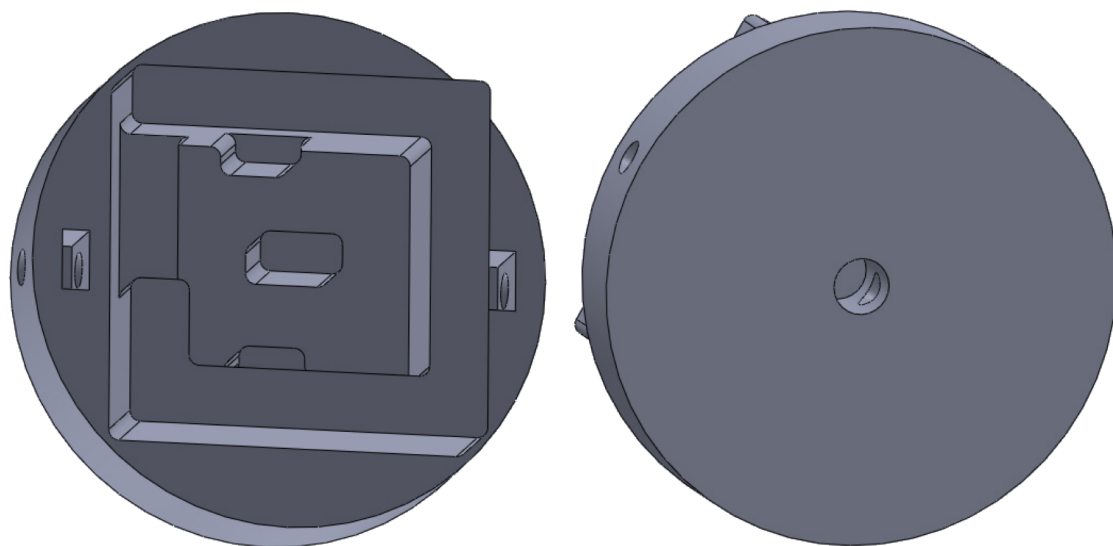


Figure F.4 – 3D view of the final piece

Then with this design, the calibration finally was successful, what means that the photodiode was illuminated from each possible direction of its FOV with a resolution of one degree.

After that, the data was stored and needed to be processed.

## Appendix G: System Requirements

Table G.1 – Requirements Glossary

<b>Field</b>	<b>Acronym</b>	<b>Description</b>
Mission	M	Related to the main goal of the system
Space Segment	SS	Related to the space segment of the mission
System	S	Related to both segments
Ground Segment	GS	Related to the ground segment
<b>Type</b>	<b>Acronym</b>	<b>Description</b>
Functional	FUNC	Related to the function
Configuration	CONF	Related to the configuration
Interfaces	INTER	Related to the interface
Physical	PHY	Related to the physical features
Environmental	ENV	Related to the environment
Quality	QA	Related to the quality
Operations	OPER	Related to the possible operations/actions
Support	SUPP	Related to the project support
Verification	VER	Related to the verification process

Table G.2 – System Requirements

Field	Type	Description
SS	FUNC	The system shall detect the light direction with an error minor than 1 °
SS	FUNC	The system PCB shall be designed with two layers
SS	ENV	The photodiode shall be placed alone in bottom layer, without any other components
SS	ENV	No vias or through-hole components shall be placed below the photodiode
SS	ENV	The op-amp should be placed alone in top layer
SS	ENV	The rest of the circuitry should be placed in the bottom layer of solar panels PCB's.
SS	ENV	The solar panels PCB's shall have a hole of the size of the photodiode (7.747 mm x 7.747 mm)
SS	PHY	The solar panels PCB's shall have a width not higher than 1.6mm
SS	FUNC	The circuit shall be connected to an ADC with a resolution equal or higher than 12 bits
SS	FUNC	The system shall process the data from the ADC
SS	FUNC	The system shall be calibrated before launch with a designed calibration system and software
SS	FUNC	The system should be calibrated using an sun simulator of the radiation Top of the Atmosphere
SS	FUNC	The system shall be tested in vacuum before launch
SS	FUNC	The system shall include a window covering the photodiode in order to achieve the specified resolution
SS	PHY	The window should be glass-made
SS	PHY	The window should be reflective
SS	PHY	The window shall have a width not higher than 1 mm
SS	PHY	The window shall have the exact same size as the photodiode (7.747 mm x 7.747mm)
SS	PHY	The window shall be attached to the photodiode using solar panels silicone
SS	INTER	The L053R8 shall include a software in order to communicate with the on-board computer via I2C.
SS	CONF	The L053R8 software shall be configurable in order to adapt power consumption.
SS	CONF	The L053R8 software shall be configurable in order to adapt the software to the timing of the requests sent from the on-board computer
SS	FUNC	The system shall have a FOV > ±50°



## **Glossary**

### **A**

AD: Analog to Digital

ADC: Analog to Digital Converter

ADCS: Attitude Control Determination System

### **D**

DMA: Direct Memory Access

DOA: Direction Of Arrival

### **E**

EPS: Electrical Power System

ESA: European Space Agency

### **F**

FOV: Field Of View

FYS: Fly Your Satellite

### **I**

I2C: Inter-Integrated Circuit

### **M**

MSB: Most Significant Bit

### **O**

OBC: On Board Computer

OLS: Ordinary Least Squares

### **P**

PCB: Printed Circuit Board

P-POD: Poly-Picosatellite Orbital Deployer

### **T**

TOA: Top Of the Atmosphere

TVAC: Thermal Vacuum Chamber